

Drivers of change in Peak Season Surface Ozone Concentrations and Impacts on Human Health over the Historical Period (1850-2014)

Steven T. Turnock^{1,2}, Dimitris Akrutidis^{3,4}, Larry Horowitz⁵, Mariano Mertens⁶, Andrea Pozzer^{3,7}, Carly L. Reddington⁸, Hantao Wang⁹, Putian Zhou¹⁰, and Fiona O'Connor^{1,11}

¹Met Office Hadley Centre, Exeter, UK

²University of Leeds Met Office Strategic (LUMOS) Research Group, University of Leeds, UK

³Max Planck Institute for Chemistry, Atmospheric Chemistry Department, Mainz, Germany

⁴Department of Meteorology and Climatology, School of Geology, Aristotle University of Thessaloniki, Thessaloniki, Greece

⁵NOAA Geophysical Fluid Dynamics Laboratory, Princeton, NJ, USA

⁶Deutsches Zentrum für Luft- und Raumfahrt (DLR), Institut für Physik der Atmosphäre, Oberpfaffenhofen, Germany

⁷Climate and Atmosphere Research Center, The Cyprus Institute, Nicosia, 1645, Cyprus

⁸Institute for Climate and Atmospheric Science (ICAS), School of Earth and Environment, University of Leeds, UK

⁹Department of Environmental Sciences and Engineering, University of North Carolina at Chapel Hill, Chapel Hill, North Carolina 27599, United States

¹⁰Institute for Atmospheric and Earth System Research (INAR), University of Helsinki, Finland

¹¹Department of Mathematics and Statistics, Global Systems Institute, University of Exeter, Exeter, UK

Correspondence: Steven Turnock (steven.turnock@metoffice.gov.uk)

Abstract. Elevated concentrations of ozone at the surface can lead to poor air quality and increased risks to human health. There have been large increases in surface ozone over the historical period associated with socio-economic development. Here the change in peak season ozone (OSDMA8) is estimated for the first time using hourly surface ozone output from 3 CMIP6 models over the 1850 to 2014 period. Additional results are obtained from one model to quantify the impact from different

5 drivers of ozone formation, including anthropogenic emissions of ozone and aerosol precursors, stratospheric ozone and climate change. The peak season ozone concentrations are used to calculate the risk to human health, in terms of the attributable fraction metric (the percentage of deaths from COPD associated with long-term exposure to elevated ozone concentrations). OSDMA8 concentrations are simulated to **increase by more than 50% more than double** across northern mid-latitude regions over the historical period, mainly driven by increases in anthropogenic emissions of NO_x and global CH₄ concentrations.

10 Small contributions are made from changes in other anthropogenic precursor emissions (CO and non-CH₄ VOCs), aerosols, stratospheric ozone and climate change. The proportion of the global population exposed to OSDMA8 concentrations above the theoretical minimum risk exposure level (32.4 ppb), increased from <20% in 1855 to >90% in 2010. This has also increased the risk to human health mortality due to COPD from long-term ozone exposure by up to 20% across Northern Hemisphere regions in the present day. Like for OSDMA8 concentrations, the drivers of the increase in the ozone health risks are attributed 15 mainly to changes in NO_x and global CH₄. Fixing anthropogenic NO_x emissions at 1850 values can eliminate the risk to human health from long-term ozone exposure in the near present-day period. Understanding the historical drivers of ozone concentrations and their risk to human health can help to inform the development of future pathways that reduce this risk.

Copyright statement. The works published in this journal are distributed under the Creative Commons Attribution 4.0 License. This licence does not affect the Crown copyright work, which is re-usable under the Open Government Licence (OGL). The Creative Commons Attribution 4.0 License and the OGL are interoperable and do not conflict with, reduce or limit each other.

20 ©Crown copyright 2024

1 Introduction

Ozone is a greenhouse gas in the troposphere and classified as a secondary air pollutant at the Earth's surface, influencing both the Earth's radiative balance and regional air quality (Szopa et al., 2021). It is formed by photochemical reactions involving 25 nitrogen oxides (NO_x), carbon monoxide (CO) and volatile organics compounds (VOCs, including CH_4) (Lelieveld and Dentener, 2000). Perturbations to the emissions associated with these precursors from both anthropogenic and natural sources can therefore alter net ozone production rates. In addition, the formation of ozone can also be impacted by geographical location and meteorological conditions such as temperature and photolysis rates (Monks et al., 2015). Furthermore, ozone concentrations at the surface are also affected by chemical destruction, surface deposition processes (Mills et al., 2018), hemispheric 30 transport (Liang et al., 2018) and the downward transport of ozone from the stratosphere (Stohl et al., 2003; Chen et al., 2024), stratosphere-troposphere exchange (STE). In air pollution episodes, exposure to elevated surface concentrations of ozone can lead to impacts on human health associated with respiratory diseases such as chronic obstructive pulmonary disease (COPD) (Pozzer et al., 2023). The Global Burden of Disease (GBD) study in 2019 estimated that long term exposure to concentrations of ozone resulted in 365,000 annual mortalities from COPD (Murray et al., 2020), with a recent revision by the GBD 35 2021 assessment to 490,000 annual mortalities in 2021 from COPD (GBD 2021 Risk Factors Collaborators, 2024). Therefore, ozone pollution represents a large current risk to the health of a population requiring an understanding of the factors controlling changes in concentrations.

Surface ozone concentrations are understood to have rapidly increased throughout the 20th Century due to industrial development and increased anthropogenic emissions of ozone precursors. Even with the uncertainties surrounding early measurements of surface ozone at the end of the 19th and beginning of the 20th Century, ozone concentrations are observed to have increased across the temperate and polar regions of the Northern Hemisphere by 30 to 70% (approximately 10 to 16 ppb) 40 since the start of the 20th Century (Tarasick et al., 2019). Previous multi-model inter comparison exercises have simulated the historical change in annual or seasonal mean tropospheric and surface ozone concentrations. In both the 5th and 6th phase of the Coupled Model Intercomparison Project (CMIP5 and CMIP6), the historical change in annual mean global surface ozone 45 concentrations from 1850 to 2000 was simulated to be in agreement at 10 to 11 ppb (Young et al., 2013; Turnock et al., 2020). Simulated historical changes in annual mean surface ozone were larger at 15 to 20 ppb across northern hemisphere mid latitude regions in both CMIP5 and CMIP6, although some regions like south and east Asia showed large inter-model diversity. However, in both phases of CMIP the simulated historical changes in surface ozone concentrations were in part dominated by the 50 large uncertainty in the simulated pre-industrial values of 1850 (Young et al., 2013; Turnock et al., 2020). Evaluating historical

changes in surface ozone concentrations is limited by the availability and reliability of observations with a sufficiently long record. Sufficient observation data is available over the last five to six decades across regions within the northern mid-latitudes (North America, Europe and Japan) and shows that both CMIP5 and CMIP6 models underestimated the recent rapid increase in surface ozone concentrations that occurred over these regions (Young et al., 2018; Parrish et al., 2014, 2021). However, the 55 CMIP6 model simulated long-term change in ozone concentrations shows good agreement when compared to the observed trend at only remote observation locations (Griffiths et al., 2021). Evaluation of the present-day simulation of ozone concentrations in CMIP5 (2000) and CMIP6 (2005 to 2014 mean) shows that both generations of chemistry climate models are able to represent the spatial and seasonal distributions of ozone but overestimate the absolute concentrations at the surface compared to ground-based observations collected as part of the Tropospheric Ozone Assessment Report (TOAR) (Young et al., 2018; 60 Turnock et al., 2020).

Dedicated model simulations allow for the studies focusing on the drivers of historical ozone changes. Generally, the most important drivers of historical ozone changes have been increases of anthropogenic emissions, especially emissions of NO_x (e.g. Lelieveld and Dentener, 2000; Fiore et al., 2009; Young et al., 2013; Turnock et al., 2018), with different emission sectors 65 having different effects on ozone due to different trends and ozone production efficiency (Dahlmann et al., 2011; Mertens et al., 2024). Besides increases in NO_x emissions, the increase of methane is also an important driver (Wild et al., 2012; Iglesias-Suarez et al., 2018; Morgenstern et al., 2018). Moreover, changes in aerosols (Xing et al., 2017), emissions of N₂O and ozone depleting substances (ODS) drive changes in tropospheric ozone (Morgenstern et al., 2018; Iglesias-Suarez et al., 2018; Zeng et al., 2022). Changes in climate via temperature, water vapor and radiation, can also influence surface ozone concentrations with increases and decreases generally anticipated in polluted and unpolluted regions respectively (Schnell et al., 70 2016; Fortems-Cheiney et al., 2017; Fu and Tian, 2019; Zanis et al., 2022). Uncertainties of various processes, such as description of natural emissions which differ in various models, however, hinders a consistent quantification of ozone drivers among various models (Archibald et al., 2020a).

75 Until lately, global estimates of ozone-attributable health impacts were based on outputs from global atmospheric-chemistry models providing surface ozone concentrations in sufficient spatio-temporal distribution for ozone exposure assessments (Anenberg et al., 2010; Lim et al., 2012; Lelieveld et al., 2015; Fang et al., 2013; Silva et al., 2013; Forouzanfar et al., 2015; Silva et al., 2016; Cohen et al., 2017; Malley et al., 2017; Liang et al., 2018; Lelieveld et al., 2020). However, as part of the first phase of TOAR, Fleming et al. (2018) provided an assessment of recent changes in relevant ozone health metrics calculated 80 from observations, showing recent reductions since 2000 across northern mid latitudes regions (North America, Europe and East Asia). More recently, the synergistic use of in-situ ozone measurements and model outputs through data fusion have made it possible to assess ozone-related health effects (Murray et al., 2020; Malashock et al., 2022) based on observational-based gridded ozone data sets (DeLang et al., 2021; Becker et al., 2023). Over the previous years different ozone exposure metrics were applied, according to the adopted coefficients from relevant cohort studies. The exposure response function (ERF) for 85 ozone is actually a mathematical formula expressing the relative risk (RR) of a disease as a function of ozone abundance.

Pope et al. (2002) and Ostro et al. (2004) introduced a log-linear ERF based on epidemiological findings, while later a log-log ERF approach was proposed Cohen et al. (2005). In the GBD 2019 report (Murray et al., 2020) a log-linear ERF was used, introducing an ozone exposure metric based on the ozone season daily maximum 8-hour mixing ratio (OSDMA8). Malashock et al. (2022), using the observation-based gridded OSDMA8 data set of DeLang et al. (2021) and the GBD2019 approach 90 for mortality calculations, reported 423,000 ozone-related deaths worldwide for the year 2019, accounting for all respiratory diseases. The review by Pozzer et al. (2023) showed that global estimates of mortality from long-term exposure to ozone have a large range from 142,000 per year from COPD to 1.3 million per year from all respiratory diseases. Although there are several 95 studies on the projected changes of ozone-related health effects under different climate change and demographic scenarios (West et al., 2007; Silva et al., 2016; Turnock et al., 2023; Pozzer et al., 2023; Akritidis et al., 2024), studies on the health effects of ozone during the historical period are lacking. In particular, few studies have quantified the change in risk to human health and the drivers behind this change over this period.

Here we make use of hourly mean surface ozone concentrations from three CMIP6 models that conducted historical transient experiments; a time resolution that has not been made available in previous global multi-model inter comparison exercises. 100 This has allowed us to calculate an ozone metric relevant to human health (OSDMA8) and explore the simulated changes in concentrations and impacts on human health over the entire CMIP6 historical period (1850 to 2014). In addition, we also use output from sensitivity experiments conducted by one of the CMIP6 models to explore the impact of changes in the different drivers of ozone formation (precursor emissions, stratospheric ozone, aerosols, climate) on the simulated concentrations and how this relates to changes in the risk to human health from long-term exposure to ozone over the same time period.

105 2 Methods

2.1 CMIP6 Model Data

We use output from the histSST experiments conducted by three different CMIP6 models as part of the Aerosols and Chemistry 110 Model Intercomparison Project (AerChemMIP), a CMIP6 endorsed Model Intercomparison Project (Collins et al., 2017). The histSST experiments were designed to be an atmosphere-only representation of the coupled historical experiment conducted by individual models using historical forcing data over the period 1850 to 2014. The three models used here, UKESM1-0-LL (Sellar et al., 2019, 2020), GFDL-ESM4 (Horowitz et al., 2020; Dunne et al., 2020) and EC-Earth3-AerChem (van Noije et al., 2021), are all global Earth system models with horizontal grid areas coarser than 100 km. All three models include an interactive representation of chemistry and aerosols, with various different couplings and feedback within the Earth system e.g. land surface, radiation etc. **All models used in this study prescribe long-lived greenhouse gases and methane as global 115 annual concentrations. Table A1 shows a brief description of relevant chemistry and aerosols processes in the three different CMIP6 models.** They are therefore suitable to use for simulating the long-term response to surface ozone from perturbations to different drivers of ozone formation, along with any feedbacks from changes in climate.

Table 1. Experiment configuration of the historical sensitivity experiments used in this study. The 3 CMIP6 models EC-Earth3-AerChem, GFDL-ESM4 and UKESM1-0-LL all provide data for histSST whereas, only UKESM1-0-LL provides data for the other experiments. Methane is prescribed as a global concentration value in these experiments. **Aerosols precursors are prescribed global emission datasets of black carbon, organic carbon and sulphur dioxide. Ozone precursors are prescribed global emission datasets of NO_x, CO, non-CH₄ VOCs. Halocarbons are prescribed global concentrations of CFC/HCFC.** Climate is represented by prescribed global datasets of sea surface temperatures and sea ice concentrations.

Scenario	Anthropogenic Air Pollutant Precursors				
	Aerosols	Ozone (non-CH ₄)	Methane	Halocarbons	Climate
histSST	Transient	Transient	Transient	Transient	Transient
piSST	Transient	Transient	Transient	Transient	Fixed at 1850
1950HC	Transient	Transient	Transient	Fixed at 1950	Transient
piAer	Fixed at 1850	Transient	Transient	Transient	Transient
piCH4	Transient	Transient	Fixed at 1850	Transient	Transient
piO3	Transient	Fixed at 1850	Transient	Transient	Transient
piNOx	Transient	NO _x only fixed at 1850	Transient	Transient	Transient
piVOC	Transient	CO and VOC fixed at 1850	Transient	Transient	Transient

Results have been obtained from UKESM1-0-LL for all the other transient historical sensitivity experiments, as this was the only model to complete all of the additional experiments requested as part of AerChemMIP (Collins et al., 2017) and thus provide hourly surface ozone concentrations. These additional sensitivity experiments involved running the historical transient simulation but with different short lived climate forcers fixed at pre-industrial values (following an "all but one" methodology), including CH₄, NO_x, CO, non-CH₄ VOCs and aerosols. A separate experiment was also conducted to consider the impact of ozone depleting substances (ODS - chlorofluorocarbons and hydrochlorofluorocarbons) on stratospheric ozone by fixing their concentrations at 1950 values. An additional experiment to those specified in AerChemMIP was conducted to examine the influence of historical climate change, where the underlying climate conditions (sea surface temperatures and sea ice cover) were kept fixed at 1850 values throughout the whole historical time period. A full list of the experiments analysed here is presented in Table 1.

Hourly mean surface ozone concentrations were obtained from each of the experiments for a single model realization over the entire historical period (1850-2014). These values were then used to calculate the relevant peak season ozone health metric (OSDMA8) by first calculating the daily maximum of 8 hour running mean values over a 24 hour period and then a 6 month running mean is calculated from these values. An annual maximum is then calculated to represent the seasonal maximum daily exposure values (avoiding biases from different peak seasons across the world), which is consistent with the metric used in the current WHO air quality guideline values (<https://apps.who.int/iris/handle/10665/345329>). Regional mean OSDMA8 values have been calculated for the 21 regions used in the GBD study (region definitions shown in Figure A1).

Surface ozone concentrations are simulated at a relatively coarse resolution (>100km) by the CMIP6 models used in this study, which can pose problems when assessing the associated impacts on air quality and human health. Additionally, previ-

140 ous evaluations have shown that global chemistry climate models tend to overestimate surface ozone concentrations (Young et al., 2018; Turnock et al., 2020). To provide a more accurate representation of surface ozone concentrations, which is necessary when linking concentrations to health effects from long-term exposure, the concentrations simulated by each model in the present day period (2005-2014) have been corrected for biases against the Regionalized Air Quality Model Performance (RAMP) dataset (Becker et al., 2023). The RAMP dataset provides a high-resolution ($0.1^\circ \times 0.1^\circ$) global surface ozone dataset
145 from 1990 to 2017 by using state-of-the-art geostatistical methods to integrate surface ozone observations with output from multiple atmospheric chemistry models (including contributions from the GFDL-AM4 model - the atmosphere model version of GFDL-ESM4). The RAMP dataset directly provides ozone concentrations as OSDMA8 values, which are used to correct the corresponding OSDMA8 values simulated by each CMIP6 model. First, each model is regressed to the finer spatial resolution of the RAMP dataset. We then use OSDMA8 values over the last 10 year mean period (2005-2014) from the RAMP
150 dataset of the historical experiments from the CMIP6 models to bias correct for the absolute difference simulated inagainst the same time period byin the CMIP6 models.RAMP dataset; Using the most recent 10-year mean period of 2005-2014 from the historical experimentswhich maximises the availability of ground-based observations in the RAMP dataset used for correction. Figure 1 shows the 10-year mean (2005 to 2014) simulated OSDMA8 values from each CMIP6 model in the histSST experiment and also the difference compared toversus the RAMP dataset in the same time period (i.e. the correction applied to
155 each CMIP6 model). EC-Earth3-AerChem shows a consistent overestimation of OSDMA8 concentrations across all regions (up to 20 ppb), whilst GFDL-ESM4 and UKESM1-0-LL have smaller underestimations and overestimations of OSDMA8 values across different regions. Applying this correction to each model for the 2005 to 2014 10-year mean period provides a present-day climatological baseline for each model that can be used as a baseline for long term changes and also in the calculation of the human health response to exposure, as the simulated concentrations align with observations now as much as
160 possible and the known biases in surface ozone concentrations have been reduced. Staehle et al. (2024) evaluateddiscuss the performance merits of four different bias correction techniques for bias correcting surface ozone in global chemistry-climate models. The techniques assessed includedincluding: mean bias, relative bias, delta correction and quantile mapping. Staehle et al. (2024) recommended using the; finding that using delta correction method for correcting future projections of surface ozoneis favourable due to its lower errors compared to mean and relative bias,performance and numerical simplicity compared
165 to quantile mapping. Delta correction has also been used as a method in other recent air pollution health studies (Akritidis et al., 2024; Pozzer et al., 2024). Therefore, based on the recommendations of Staehle et al. (2024) and other recent studies, we use the delta correction method to calculate the change in historical ozone concentrations by applying the ratio of change between each decadal mean and the present day (2005-2014) on top of the bias corrected baseline for each model. This then generates a new historical time series for each experiment that is connected to the observed present day values. The temporal
170 changes in OSDMA8 values (from histSST) are calculated by comparing each 10-year mean period to the 2005-2014 baseline period. Whereas, Tthe contribution of each individualimpact of the historical drivers is obtained through a comparison of different pairs of bias corrected model experiments i.e. a control experiment (histSST) with an individual (sensitivity experiment where an individual driver is fixed (e.g. p_1NO_x).s) The contribution of each individual driver is calculatedassessed by taking the difference between OSDMA8 concentrations in the samecomparing the 10-year mean time period between each of these

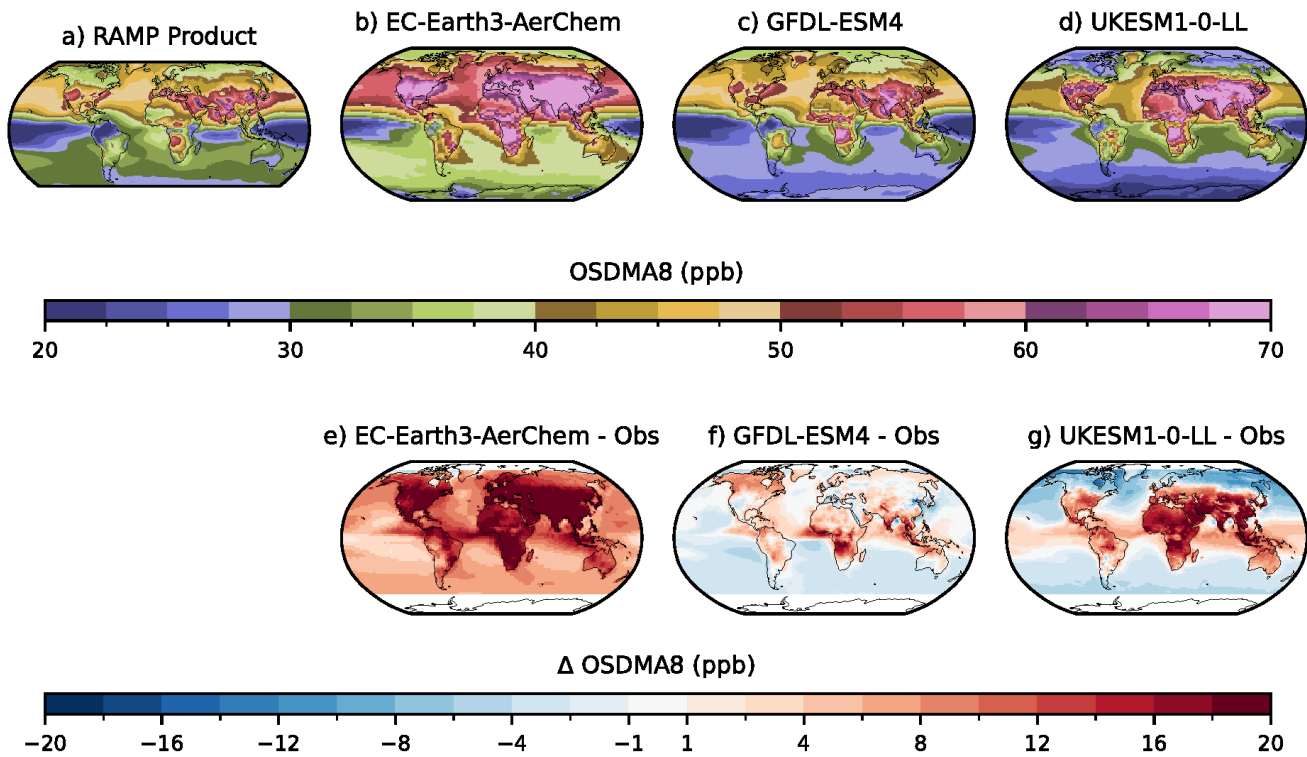


Figure 1. 10 year mean surface OSDMA8 values (2005 to 2014) from the a) RAMP observational dataset (Becker et al., 2023) and simulated by 3 CMIP6 models ba) EC-Earth3-AerChem, cb) GFDL-ESM4 and de) UKESM1-0-LL and difference in the same models ed) to gf) when compared to the RAMP observational dataset (Becker et al., 2023) over the same time period.

175 paired experiments. For example, to quantify the contribution of NO_x emissions to OSDMA8 concentrations values in the 2005 to 2014 time period, the 10-year mean OSDMA8 values in this time period from the piNO_x experiment (where NO_x emissions are fixed at 1850 values) are subtracted from the values in the same time period of in the histSST experiment experiment (where NO_x emissions have changed) i.e. histSST minus piNO_x . This example quantifies the change in OSDMA8 concentrations in the 2005 to 2014 time period to NO_x emissions if they had increased from 1850 to 2014 values. This method is then repeated
 180 for each individual driver using the relevant control and sensitivity experiment pairs. to the same time period in each of the sensitivity simulations:

A feature of the histSST sensitivity experiments conducted by UKESM1-0-LL is that they use prescribed values of global CH₄ concentrations, which are unable to respond to any other perturbation of the inputs (e.g., fixing NO_x emissions at 1850 values), in the same way as a CH₄ emission-driven model would. This experimental set up therefore neglects the impacts of any of the sensitivity experiments on global CH₄ concentrations and also consequently ozone, as CH₄ is a precursor to ozone formation. Therefore, in each of the histSST sensitivity experiments we have adjusted the ozone concentrations to take account for the consequences of changes in the CH₄ lifetime (from the feedback on its own concentrations). Firstly, a global CH₄ lifetime is calculated for each experiment, including histSST. The CH₄ feedback factor (Prather, 1996) is then calculated by using the difference in the CH₄ lifetime and CH₄ concentrations in the histSST and histSST-piCH4 experiments over the 30-year period 1930 to 1960, when large changes in CH₄ concentrations occur but there are smaller influences from other factors, e.g., halocarbons (Stevenson et al., 2020). The CH₄ feedback factor is calculated to be 1.30 over this 30-year period, which is similar to other previous estimates (O'Connor et al., 2021; Stevenson et al., 2013). The feedback factor and CH₄ lifetime can then be used to calculate the equilibrium CH₄ concentrations in each experiment from the transient prescribed values used. The difference in prescribed and equilibrium CH₄ concentrations can be used as input to the relationship between CH₄ perturbations and ozone response derived by Wild et al. (2012) and subsequently updated by Turnock et al. (2018). This relationship was obtained by analysing the ozone response of multiple chemistry transport models in an experiment where the global CH₄ concentrations was reduced by 20%; conducted as part of phase 1 and 2 of the Hemispheric Transport of Air Pollutant (HTAP) project. A non-linear relationship is then used to scale this ozone response (calculated from the HTAP 20% global CH₄ reduction experiment) by the ratio of the global CH₄ abundance change in this study (the difference between equilibrium and prescribed concentrations) relative to the 20% abundance change used in the original HTAP experiments. From this we nowUsing this relationship, we calculate for each sensitivity experiment the response in surface ozone concentrations that occurs due to the change in CH₄ concentrations resulting from the adjustment of CH₄ lifetime. The model simulated ozone concentrations are then adjusted accordingly in each of the histSST sensitivity experiments for this change. Four of the sensitivity experiments (piSST, 1950HC, piNOx and piO3) result in an increase in CH₄ concentrations and subsequently a relatively small increase in ozone. Whereas, in the other three sensitivity experiments (piAer, piCH4 and piVOC) there is a small reduction in CH₄ and ozone concentrations. The magnitude of adjustment to the ozone response slightly varies across regions in each sensitivity experiment, although the sign of change is the same. These ozone values adjusted for the impact of CH₄ lifetime can then be used to calculate the historical changes in surface ozone values relative to the bias-corrected baseline period.

2.2 Emissions in Historical Scenarios

There have been large changes in emissions of ozone precursors (CO, NO_x, non-CH₄ VOCs and CH₄) since 1850 due to increasing human industrial activity and economic development (Hoesly et al., 2018). Figure 2 shows the relative change (compared to 1850 values) in these ozone precursors that are used as input to the CMIP6 historical experiments and sensitivity experiments considered in this study (Table 1). Global anthropogenic emissions of NO_x have seen the largest increase

of the ozone precursor emissions, a ~~fractional increase of >10~~~~factor of >11~~ increase globally since 1850. Global emissions of non-CH₄ VOCs and CO, along with global CH₄ concentrations have all increased globally by a ~~fractional change~~~~factor~~ of ~~>1 (i.e. more than doubled)~~~~2~~ since 1850. These large changes will all have a substantial effect on surface ozone concentrations throughout the historical period considered in the CMIP6 experiments (1850 to 2014). Additionally, changes in climate and stratospheric ozone concentrations over the historical period will also have an influence on surface ozone concentrations; the changes in these are considered in the sensitivity experiments in Table 1. The transient change in surface air temperature simulated by UKESM1-0-LL over the historical period (Fig. 2 right panel) showed particularly large cold biases compared to observations throughout the latter half of the 20th Century (peak of ≈ 0.5 k), which was similar to a number of other CMIP6 models (Flynn and Mauritsen, 2020). The cold temperature biases simulated by UKESM1-0-LL have been previously attributed to an excessive aerosol forcing, with recent changes to aerosol and cloud properties in an updated version (UKESM1-1-LL) showing an improved representation of historical surface temperatures (Zhang et al., 2021; Mulcahy et al., 2023). However, in 2014 the global annual mean surface temperature in HadCRUT5 observations (Morice et al., 2021) and UKESM1-0-LL simulations (Fig. 2) both increased by a similar amount of ≈ 1 K (compared to a 1850 to 1900 mean period), mainly due to increasing concentrations of long-lived greenhouse gases (Chen et al., 2021). Total column ozone burdens have shown large reductions since the 1960s in UKESM1-0-LL historical simulations due to the reductions in stratospheric ozone from increases in ozone depleting substances, e.g. CFCs. However, total column ozone simulated by UKESM1-0-LL in CMIP6 simulations tends to be higher than other CMIP6 models and observations, and also simulates a stronger depletion of stratospheric ozone from 1960 to 2000 (Keeble et al., 2021). All of these drivers of surface ozone are used as transient changes to the inputs for the histSST experiment and are also fixed at 1850 values (or 1950 for ODS) for the individual sensitivity experiments.

2.3 Health Calculations

To assess the health impacts from long-term exposure to ozone concentrations during the historical period, we use the attributable fraction (AF) metric, which is defined here as the percentage of deaths from chronic obstructive pulmonary disease (COPD) attributable to ozone pollution. A full health assessment is not undertaken due to the absence of long term datasets for changes in population (on a latitude longitude grid) and country specific baseline mortality rates over the 1850 to 2014 period. In more detail, AF(x,y,t) is calculated at a given location with x and y coordinates and for a specific time period t, as shown in equation (1):

$$245 \quad AF(x, y, t) = \frac{RR(x, y, t) - 1}{RR(x, y, t)} \quad (1)$$

where RR(x,y,t) is the relative risk (also known as hazard ratio) for ozone-related excess mortality from COPD. Following the GBD 2019 methodology (Murray et al., 2020), RR is estimated using a log-linear function as shown in equation (2):

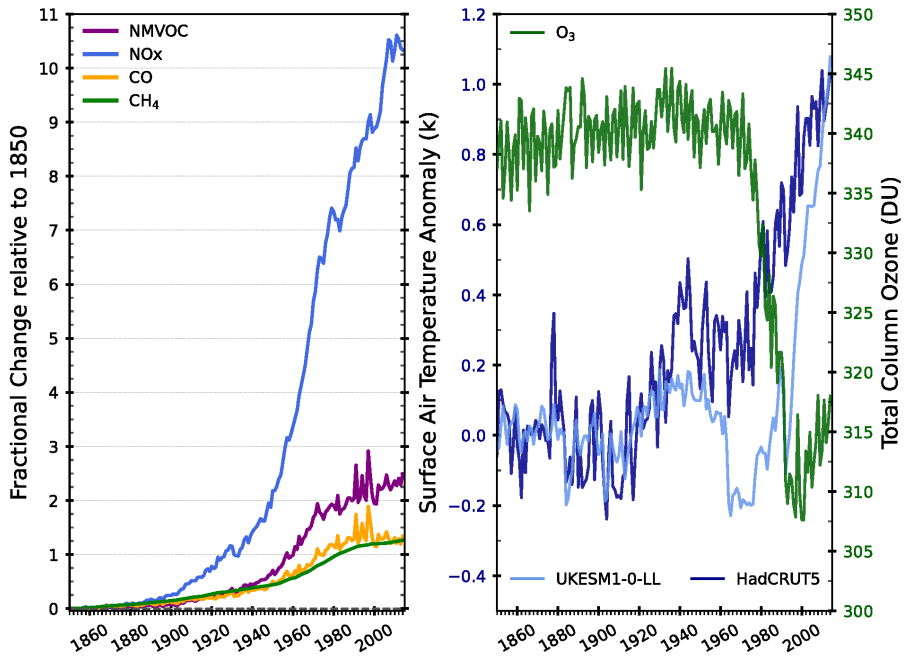


Figure 2. Relative change in total historical emissions of ozone precursors (NO_x , CO and NM(non- CH_4)VOCs) and global CH_4 concentrations compared to 1850 values (left panel). Global annual mean surface air temperature anomaly, relative to an 1850–1900 mean period, from UKESM1-0-LL historical simulations and HadCRUT5 (Morice et al., 2021) (blue lines, right panel). Global annual mean total column ozone values from 1850 to 2014 simulated by UKESM1-0-LL (green line, right panel).

$$RR(x, y, t) = e^{\beta(X(x, y, t) - TMREL)} \quad (2)$$

250 where $X(x, y, t)$ is the health-relevant ozone metric (OSDMA8) at the given location and time period and TMREL is the theoretical minimum risk exposure level, below which ozone is considered as not being harmful for human health. For TMREL we adopted the value of 32.4 (29.1–35.7) ppb, while the β parameter value(s) result from the RR per 10 ppb of ozone (OSDMA8) value of 1.063 (1.029–1.098), estimated from a meta-regression of five cohorts studies (Murray et al., 2020).

255 Since ozone concentrations (OSDMA8) are the only varying input in the AF calculations, the AF temporal changes over the historical period reflect the changes of the percentage of ozone-related COPD excess mortality from ozone variations only. The ozone exposure values were calculated as 10-year mean OSDMA8 values across the historical period from the bias-corrected model simulation data. An assessment of population exposure to ozone is also provided by calculating the number of people exposed to OSDMA8 concentrations concentrations above the TMREL in 3 different decadal time periods (1850–59, 1980–89

260 and 2005-142010). Population data for these periods is obtained for the nearest available years (1850, 1980 and 2010) from the Hyde dataset Hyde (History database of the Global Environment) (Klein Goldewijk et al., 2017).

265 Attribution of ozone health effects (AF) to different drivers by taking the difference between the reference and sensitivity simulations is not valid, as AF is not directly proportional to OSDMA8 concentrations but rather depends on whether ozone exceeds the TMREL and by how much. This type of decomposition would be feasible if the actual percentage contribution of each driver to the total OSDMA8 change could be estimated, which is not possible in the current approach due to the non-linearity in ozone chemistry. Therefore, only qualitative insights can be made on the relative contributions of each driver to ozone health effects. Thus, AF in a sensitivity simulation should be viewed as a conceptual indicator, reflecting the potential health impacts under a specific scenario (e.g., pre-industrial NO_x emissions in near present-day conditions), without providing a direct attribution of the health effects of ozone to individual drivers in the real-world context.

270 3 Results

3.1 Multi-model Historical Changes in Surface Ozone and Risk to Human Health

3.1.1 Multi-model Historical Changes in OSDMA8

275 The regional mean change in OSDMA8 concentrations over the 1850 to 2014 period from the 3 bias-corrected CMIP6 models is shown in Figure 3. Large changes in OSDMA8 concentrations have been simulated across all regions over the historical period. Globally, the 10-year multi-model mean (+/- 1 S.D. of 3 model values) OSDMA8 concentrations are simulated to have increased by 12 +/- 2.6 ppb (50% increase) between 10-year mean values centered on from 1855 and to 2010, which is of similar magnitude to annual mean changes simulated by 6 CMIP6 models (Turnock et al., 2020) and also other previous global chemistry climate model intercomparison studies (Young et al., 2013). In addition, this simulated historical change in global OSDMA8 is within the observed change of surface ozone across the Northern Hemisphere of 30 to 70 % (approximately 10 280 to 16 ppb) from Tarasick et al. (2019). The largest regional mean increases over the same time period have been simulated to occur over South Asia (29.8 +/- 5.3 ppb, 115%), East Asia (24.8 +/- 2.2 ppb, 88%), High-income Asia Pacific (24.8 +/- 0.4 ppb, 110%), North Africa and Middle East (21.4 +/- 4.8 ppb, 78%), Central Europe (21.3 +/- 3.9 ppb, 90%) and High-income 285 North America (18.6 +/- 1.9, 81%). Previously, CMIP6 models were shown to be able to represent the multi-decadal changes in surface ozone concentrations since 1960 at five remote long-term monitoring remote locations around the world (Griffiths et al., 2021). Even though this comparison is spatially limited, due to the availability of monitoring locations with multi-decadal observational records, it does provide a degree of providing confidence in the ability of models to simulate long-term changes at specific remote locations, representative of background conditions. Across most regions OSDMA8 concentrations only show small increases up until about 1950. After this time period concentrations rapidly increase (by approximately 50% 290 more than doubling) to 2005-2014 values, driven by the large rapid changes in all anthropogenic precursors of ozone (CH₄, NO_x, CO, Non-CH₄ VOCs), with the largest relative changes occurring in NO_x emissions (Fig. 2). The increase in concentrations continued across certain regions, most notably South Asia, East Asia and other tropical and sub-tropical regions, due

to the continued increases in anthropogenic ozone precursors from socio-economic development across these regions (Figure A3). However, across some regions in the northern mid-latitudes (high-income North America, Europe and high-income Asia Pacific) OSDMA8 concentrations stopped increasing from about the 1980s, remaining at and near these values until the end 295 of the CMIP6 historical period when a slight reduction in concentrations occurred, in agreement with the observations in the RAMP dataset (Fig. 3). The recent change in OSDMA8 concentrations is consistent with the mitigation measures adopted over these regions to improve regional air quality by reducing primary air pollutant emissions (United Nations Economic Commission for Europe, 2004; EMEP Steering Body and Working Group on Effects of the Convention on Long-Range Transboundary Air Pollution, 2016), shown by a reduction in NO_x emissions from the peak in the 1980-1990s (Figure A3).

300

Fig. 3 shows that bias correcting the model data to the RAMP dataset has resulted in the simulated OSDMA8 concentrations from all 3 models being similar in the 2005 to 2014 10-year mean period. However, there is still a diversity of 10 to 15% in the model simulated OSDMA8 concentrations in the pre-industrial period (1850 to 1860), with some of the largest model differences (20%) occurring over South Asia. UKESM1-0-LL consistently simulates larger bias-corrected OSDMA8 concentrations 305 across most regions in the first 10 year mean period of 1855, with GFDL-ESM4 tending to have the lowest concentrations of the 3 models. **This diversity between models can be attributed to differences in how they represent chemical processes (see Table A1), particularly relevant for the pre-industrial period are differences in the representation of meteorology/climate, as well as the interactive/natural components such as emissions from biogenic sources (BVOCs), lightning NO_x and wetland CH₄ (Rowlinson et al., 2020; Wild et al., 2020)** In addition, differences in resolution (both horizontal and vertical) and chemical 310 mechanisms between each of the models can also contribute to the highlighted diversity in simulated ozone concentrations (Wild and Prather, 2006; Wild et al., 2020). These structural differences between models also impacts **This diversity, along with differences in** the chemical sensitivity of ozone formation in each model, resulting in the different simulated historical changes in OSDMA8 across the models (Turnock et al., 2020). Given its higher 1855 concentrations, UKESM1-0-LL is the model that tends to simulate the smallest historical change in OSDMA8 values over the historical period (9.2 ppb globally), 315 whilst GFDL-ESM4 simulates the largest (14.3 ppb globally). If the models are not corrected against the observation based dataset then the simulated concentrations show on average a larger 20% variability between models (up to 30% across South Asia), with the largest diversity in concentrations in the 1855 period. The comparison to the RAMP dataset in the 2005 to 2014 period shows that simulated OSDMA8 values tend to be consistently overestimated by all 3 models (Fig. 1, Figure A2). Over-estimating OSDMA8 concentrations has important consequences for the assessment of the long-term impact on human health 320 due to the use of theoretical minimum risk exposure level, below which no risk to health is considered (Section 2.3). Using the uncorrected simulated OSDMA8 concentrations from the models could result in an overestimation of the impacts to human health from long-term exposure, and thus the bias-corrected model simulated concentrations are used for any assessment of health impacts.

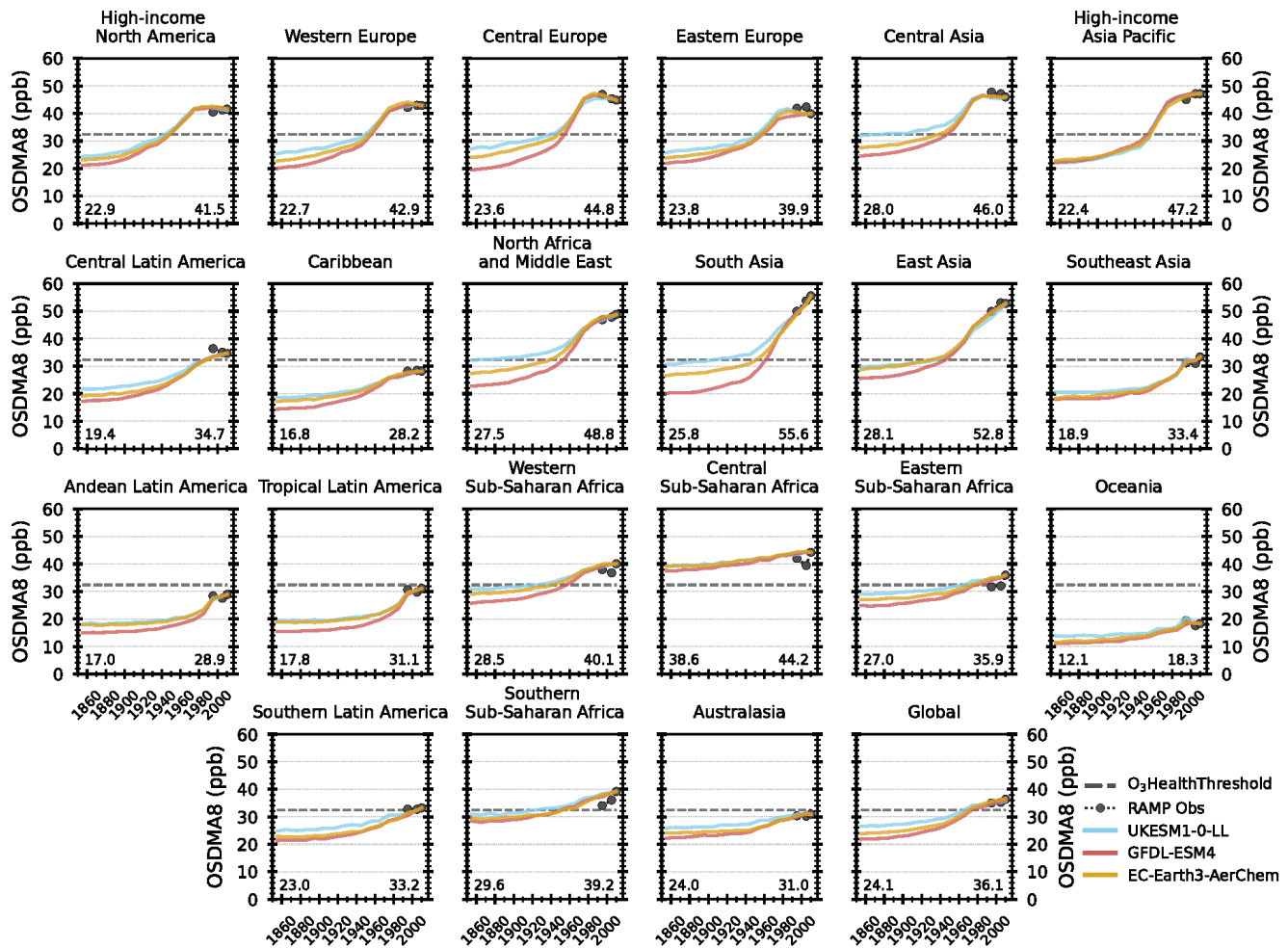


Figure 3. Regional mean surface OSDMA8 values from 3 CMIP6 models simulated over the historical period (1850-2014) bias-corrected to a 10-year mean of observations from Becker et al. (2023). Observations from Becker et al. (2023) are shown as circles on each relevant region with the TMREL value of 32.4 ppb as the dashed line. **Regional multi-model mean OSDMA8 values are shown for the start and end of the time period.**

325 3.1.2 Historical Changes in Ozone exposure and risk to Human Health

The increase in OSDMA8 concentrations over the historical period across all regions has increased the risk to human health via enhanced long-term exposure to ozone. Figure 3 shows how the simulated regional OSDMA8 concentrations compare with the TMREL of 32.4 ppb. All three models simulate concentrations in first 10-year mean period of 1855 that are below this threshold across most regions of the world, resulting in <20% of the world's population in 1850 being exposed to concentrations above 330 this value (Fig. 4a). However, the simulated increase in OSDMA8 concentrations over the historical period has resulted in concentrations being above the TMREL value in almost every region of the world in the near present-day period. This is shown by

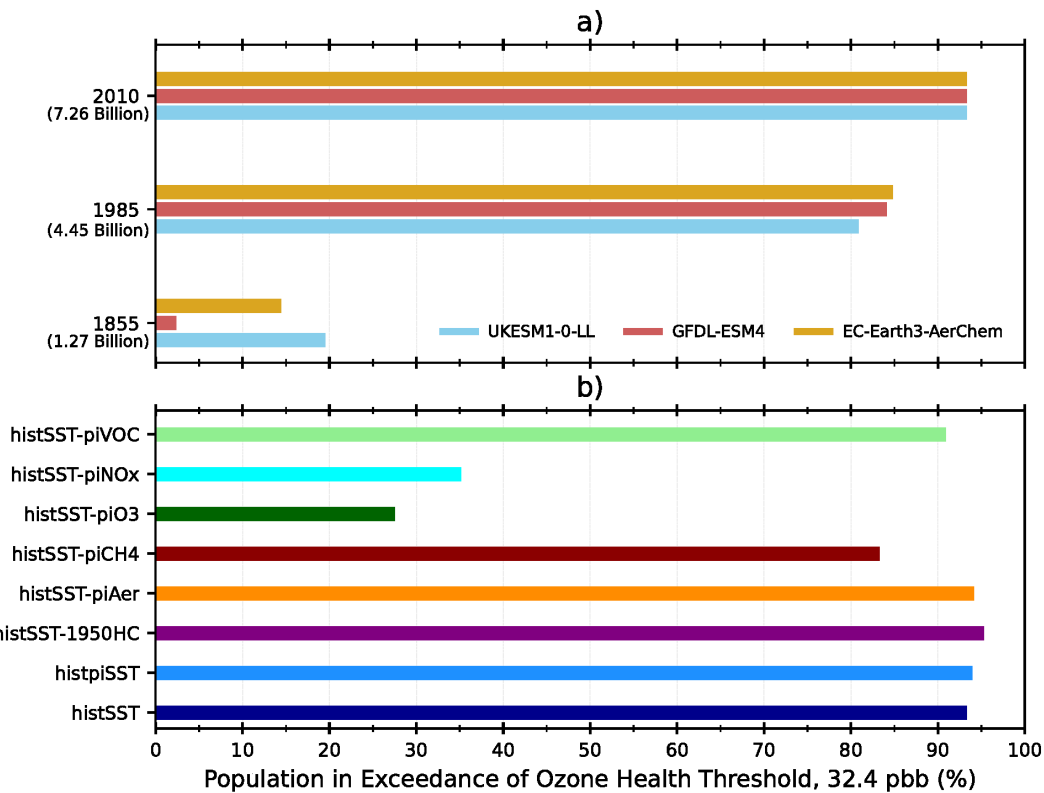


Figure 4. Percentage of total global population in exceedance of the theoretical minimum risk exposure level (TMREL - 32.4 ppb) to ozone across 3 historical time periods from 3 different CMIP6 models a) and in the different present day (2010) for sensitivity scenarios with different drivers of ozone fixed b). Total global population for each time period is shown in parenthesis on a).

>90% of the world's population in 2010 being exposed to ozone concentrations above this value, meaning that over the historical period there has been a large increase in the risk to human health from long-term exposure to elevated ozone concentrations.

335 Figure 5 shows the spatial distribution of the multi-model mean attributable fraction over the pre-industrial period 1850-1859 and the near present-day period 2005-2014. High AF values up to $\approx 20\%$ are found over regions of North India, East China, Middle East, and Western United States, indicating that across these regions approximately one out of five COPD deaths in the near present-day period are attributed to long-term ozone exposure. High AF values of $>8\%$ also occur over Greenland in 2005-2014, which can be attributed to the presence of the high-altitude ice sheet ($\approx 2000\text{m}$ above sea level), meaning that 340 the ozone concentrations are not representative of typical surface values for this latitude but can be considered more like elevated free-tropospheric ozone concentrations. As the AF calculation does not consider changes in population and baseline mortality rates, a distinct increase of the AF is depicted almost globally compared to the 1850-1859 period due entirely to increases in ozone concentrations. As ozone concentrations in the pre-industrial period are below the TMREL value almost all over the world, the respective AF values are near zero. The major exception to this is that AF values are approximately

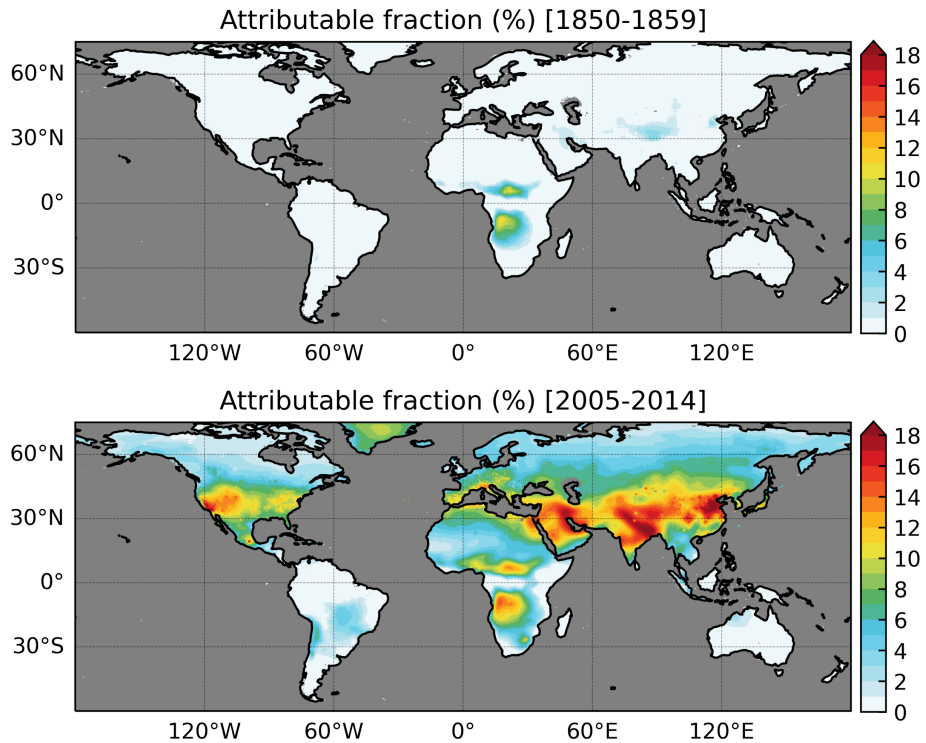


Figure 5. Attributable fraction as the percentage of deaths from COPD attributable to ozone pollution calculated from the multi-model mean OSDMA8 values in the 10 year mean periods of 1850-1859 (top) and 2005-2014 (bottom).

345 5% in the 1850-59 period over the Central Sub-Saharan Africa region. This non-zero AF is due to the elevated pre-industrial
 OSDMA8 concentrations (Fig. 3) arising mainly from biomass burning sources of ozone precursors over this region in this
 period, although the low population density in this region and time period would represent a low risk to health. Overall this
 suggests that there is no risk for human health from ozone exposure in the pre-industrial period, although the increases in ozone
 concentrations up to the near present-day became a major threat for human health, being responsible for more than 10% of
 350 COPD deaths in many regions of the Northern Hemisphere.

3.2 Drivers of Historical Change in Surface Ozone and Risk to Human Health

3.2.1 Drivers of Historical Change in OSDMA8

Figure 6 shows the change in OSDMA8 concentrations in the present day time period (2005 to 2014) due to the historical changes in **all drivers together (histSST)** and due to the individual drivers of ozone formation i.e. histSST minus sensitivity experiment. The overall change in global mean OSDMA8 concentrations simulated by UKESM1-0-LL over the historical period in histSST is 9.2 ppb. Considering only historical changes in emissions of ozone precursors (i.e., histSST minus histSST-piO3 = NO_x , CO and non- CH_4 VOCs) has resulted in a large increase in global mean OSDMA8 concentrations of 9.6 ppb (37%)

in the 2005 to 2014 mean period. Of these three precursors, the majority of this change in global mean OSDMA8 concentrations in 2005-14 can be attributed to historical changes in anthropogenic NO_x emissions (8.6 ppb, 32%), compared to CO and 360 non-CH₄ VOCs (1.5 ppb, 4%). Regionally, the largest changes in OSDMA8 concentrations occur mainly over the polluted continental regions of the northern mid-latitudes. OSDMA8 concentrations increased by more than doubled (≈ 25 ppb) over the High-income Asia Pacific region, due to this region having the largest relative increase in anthropogenic NO_x emissions over the historical period (Figure A3). Similarly large increases in OSDMA8 concentrations occur over Europe (16 ppb), High-income North America (16 ppb), East Asia (23 ppb) and South Asia (24 ppb), all mainly due to the large historical changes 365 in anthropogenic NO_x emissions over these regions (Figure A3). Changes in anthropogenic emissions of ozone precursors, particularly over recent decades have also been shown, as in this study, to be the most important driver behind changes in regional surface ozone concentrations (Parrish et al., 2014; Zhang et al., 2016; Lin et al., 2017; Yan et al., 2018; Wang et al., 2022).

370 Historically, global CH₄ concentrations, the other major precursor gas to ozone formation, have more than doubled increased by a factor of ≈ 2 since 1850 (Fig. 2), which has increased global mean OSDMA8 concentrations by 5.9 ppb (20%) in the 2005 to 2014 period. The impact of changes in CH₄ on surface ozone concentrations tends to be larger, in emissions and abundance, than other non-methane VOCs and to be more globally uniform due to its larger change over the historical period, the longer 375 chemical lifetime of CH₄, its larger abundance in the atmosphere, and that it is input to these model experiments as a global annual mean concentration, rather than gridded emissions. This means that the impact of changes in CH₄ on surface ozone in this study are spatially limited by the absence of a hemispheric gradient in CH₄ concentrations (higher in the northern hemisphere and lower in the southern hemisphere), something that would be provided if using a model with a fully interactive CH₄ cycle, including CH₄ emissions instead of concentrations (Folberth et al., 2022). The largest increase in OSDMA8 concentrations occurred over parts of Asia and North Africa and Middle East (up to 8.5 ppb, 21%), whilst the smallest increase (2 380 to 3 ppb, 10 to 13%) occurred over tropical regions of the southern hemisphere. Over some of these more remote (low NO_x) regions like sub-Saharan Africa and southern Latin America, historical changes in CH₄ had a larger proportional impact on OSDMA8 concentrations, contributing almost as much as changes in NO_x emissions. This shows that historical changes in CH₄ concentrations have been important in altering the background ozone concentrations in most regions of the world.

385 The other drivers of surface ozone formation considered here in the sensitivity experiments are historical changes in climate, aerosols and stratospheric ozone via ODS, which have all tended to have smaller impacts than anthropogenic ozone precursor emissions (Fig. 6 and Figure A4 for more detail). The increasing emissions of ODS since the 1950s reduced stratospheric ozone concentrations (shown as total ozone column on Fig. 2) significantly by the start of the 21st Century, which has also led 390 to reductions in OSDMA8 concentrations, potentially via less downward transport to the surface or from changes to photolysis rates. Global mean OSDMA8 concentrations reduced by -2.8 ppb (-7%) in the 10-year mean period of 2005 to 2014 period due to smaller amounts of stratospheric ozone from the increased ODS in the histSST experiment compared to the 1950HC experiment in this most recent period. Some of the largest impacts (>2 ppb) occurred over remote southern hemisphere regions,

including southern Latin America and Australasia (Figure A4). In addition, changes in stratospheric ozone also reduced OSDMA8 concentrations across the well known hot spots regions of stratosphere-to-troposphere transport (STT) (Škerlak et al., 395 Akritidis et al., 2021) of high altitude Central Asia, the Eastern Mediterranean and Middle East, and the Western United States.

Increasing emissions of aerosols and aerosol precursors over the historical period (Figure A5) has resulted in a small reduction of global mean OSDMA8 concentrations of -0.8 ppb (-2%) in the 2005 to 2014 period (see Figure A4 for more detail). 400 Increasing aerosols over the historical period implies that there is an increase in the heterogeneous loss of nitrogen oxides to aerosol surfaces (the only active heterogeneous tropospheric mechanism currently in UKESM1-0-LL (Archibald et al., 2020b)), leading to a reduction in ozone formation. This effect is probably underestimated due to the absence of the loss mechanism involving HO₂ uptake on aerosols in UKESM1-0-LL (Ivatt et al., 2022). Regionally, increasing aerosols causes the largest 405 reduction in OSDMA8 concentrations of up to -2.1 ppb (-4%) across Asia (central, south and east), North Africa and Middle East regions in the 2005 to 2014 period when aerosol concentrations were higher. However, the largest reduction on OSDMA8 concentrations from aerosols (-2.7 ppb, -6%) occurred in the 1980s across Europe. Aerosol concentrations peaked in Europe at this time due to the subsequent enacting of air pollutant controls, meaning aerosol concentrations and their impact on surface ozone were reduced thereafter (Turnock et al., 2015).

410 The climate change signal over the historical period has resulted in an approximate 1K increase in global mean surface temperatures simulated by UKESM1-0-LL by the 2005 to 2014 period (Fig. 2), which has resulted in a small reduction in global mean OSDMA8 concentrations of -0.8 ppb (-2%) **that is consistent with the surface ozone temperature sensitivity of -0.79 ppbv °C⁻¹ from Zanis et al. (2022)**. The global mean reduction in ozone has mainly been driven by decreases over the ocean, which can be attributed to more ozone destruction here due to increased hydroxyl formation from enhanced amounts of 415 water vapour occurring in a warmer world (Johnson et al., 1999; Doherty et al., 2013; Zanis et al., 2022). Historical climate change has resulted in enhanced ozone formation rates over some polluted continental regions **including** including Southeast Asia, Central Europe, east Asia, high-income Asia Pacific and parts of North America (see Figure A4 for more detail), which is shown by a small increase of OSDMA8 concentrations (<1 ppb, 2%). There has also been a similar small increase in OSDMA8 concentrations across some of major biogenic emission regions (Central Sub-Saharan Africa and parts South America).**;** This 420 **suggestsing** a small climate impact on natural sources of ozone precursor emissions **is simulated by the interactive BVOC emission scheme included within UKESM1-0-LL**. The magnitude of the changes in ozone due to 1K of warming over the historical period are consistent with studies analysing the change of ozone in response to future warming (Archibald et al., 2020c; Zanis et al., 2022), with the impact of climate change on surface ozone being less in this study due to the smaller level of historical warming compared to those projected for **thea** future warming of 2.7 to 5.4K. In addition, Zanis et al. (2022) 425 showed that UKESM1-0-LL had a lower ozone sensitivity per unit temperature change on a global mean basis (-0.79 ppbv °C⁻¹) than other CMIP6 models (multi-model mean of -0.93 ppbv °C⁻¹), which could mean that climate change impacts on surface ozone are underestimated in this study. However, this global sensitivity number obscures the spatial variation in the

430 sensitivity of surface ozone to temperature (both positive and negative) across different models (Zanis et al., 2022). The model diversity highlights that the surface ozone response to climate change is still uncertain in global chemistry climate models and that both a stronger and weaker response is possible across different regions.

In summary, the model experiments isolating the impact of the individual drivers shows that historical changes in anthropogenic NO_x emissions contribute the most, approximately 42%, to the summed total change in historical global mean OSDMA8 concentrations from all drivers combined. The contribution to historical changes in global mean OSDMA8 concentrations from other drivers was 29% from global CH₄ concentrations, 14% from stratospheric ozone, 7% from anthropogenic emissions of CO and non-CH₄ VOCs, and 4% from both aerosols and climate change. This attribution of drivers is in agreement with other studies that showed the reductions in peak season surface ozone over North America and Europe and increases over east and south Asia between 1980 and 2010 were primarily driven by changes in anthropogenic ozone precursor emissions, with much smaller contribution from other factors including changes in CH₄ concentrations and climate (Zhang et al., 440 2016; Yan et al., 2018; Wang et al., 2022). However, the linear combination of the historical change in global mean OSDMA8 concentrations, calculated from the individual driver experiments by UKESM1-0-LL (+11.6 ppb), is found to be about 20% larger than that calculated when all drivers are varied simultaneously (+9.2 ppb from histSST). This indicates at a global scale that there are feedbacks and interactions (e.g., clouds or aerosols influencing photolysis rates) influencing ozone important 445 non-linearities in the formation in each of the individual experiments due to the changes from that particular driver (Gao et al., 2020; Qu et al., 2021) of ozone from the interactions between the different drivers. These feedbacks/interactions then have a non-linear effect on the formation of ozone, reducing the magnitude of change in OSDMA8 at the global scale when the drivers are changed in combination in single experiment (histSST). At the global scale, the impact on ozone concentrations due to each individual driver can be considered overestimated as change in the combined driver experiment (histSST) is smaller than those from the linear addition of the individual driver experiments.

450

3.2.2 Drivers of change in Ozone Exposure and risk to Human Health

The change in the individual drivers of ozone formation show different impacts of OSDMA8 concentrations over the historical period, which will also have an impact on the risk to human health via changes to long-term exposure. Figure 4b) shows a comparison of the different fraction of the global population in 2010 that are exposed to OSDMA8 concentrations above the 455 TMREL of 32.4 ppb in each of the sensitivity scenarios that isolate the different drivers of ozone formation. If emissions of ozone precursors (NO_x, CO and non-CH₄ VOCs) are kept fixed at 1850 values then the fraction of the near present-day global population exposed to OSDMA8 concentrations above 32.4 ppb is reduced substantially to 27%, from >90% when emissions are allowed to increase in histSST. Fixing solely anthropogenic NO_x emissions at 1850 is shown to be the dominant cause of this reduction by decreasing the global population exposure above the TMREL to 34%. Fixing the emissions of the other 460 precursors (CO and non-CH₄ VOCs) at 1850 values results in a very small (2%) change in global population exposure. A relatively small impact on global population exposure is shown when fixing global CH₄ concentrations at 1850, which reduces the

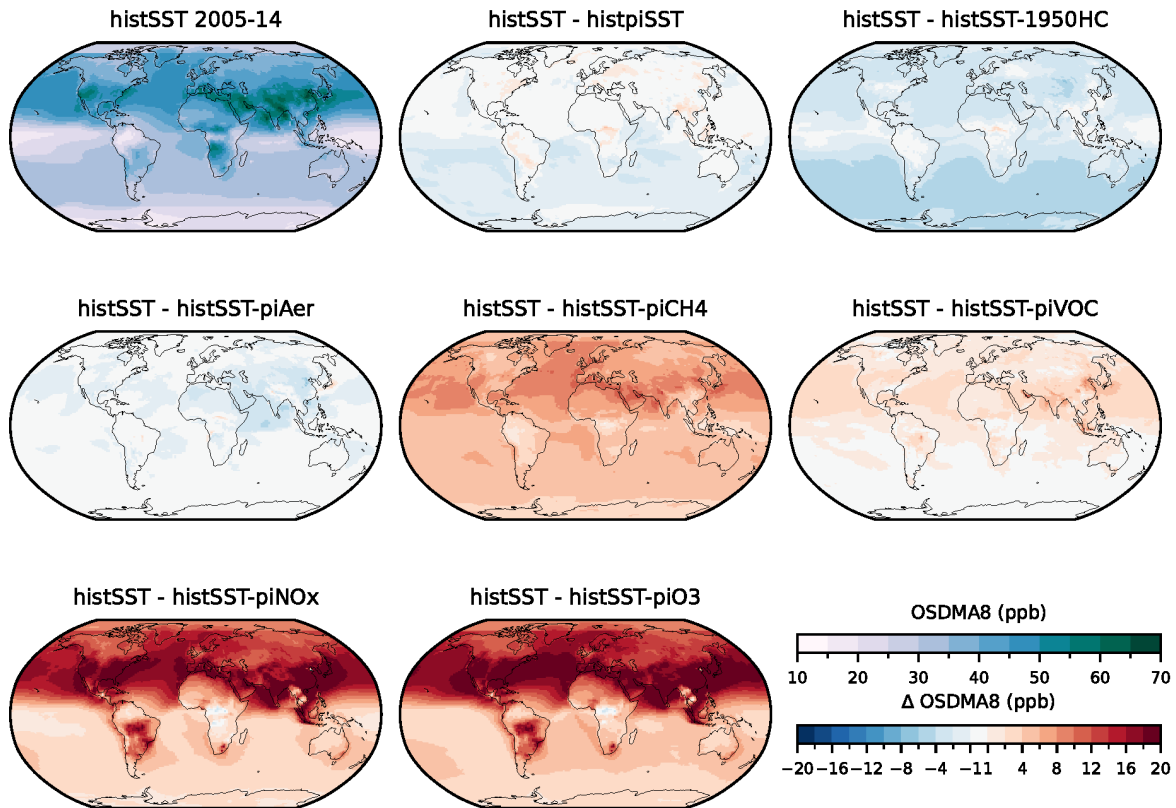


Figure 6. 10-year mean in surface OSDMA8 values simulated by UKESM1-0-LL in the HistSST experiment for 2005-14 (bias-corrected) and the change in the same time period in the HistSST experiment relative to each of the sensitivity experiments with different drivers of ozone fixed

proportion of the global population exposed to OSDMA8 **concentrationseones** above TMREL to 83% (from >90%). Fixing the other historical drivers of ozone concentrations (climate change, stratospheric ozone and aerosols) slightly increases the global population exposure to OSDMA concentrations above the TMREL by 1 to 2%. These results show that historical changes in 465 anthropogenic NO_x emissions are the leading cause of increased ozone exposure that is considered harmful to human health.

Figure 7 presents the **global and regional mean AFsattributable fraction** for the histSST and **the** sensitivity experiments isolating the different drivers of ozone formation **infor** the near present-day period 2015-2014. **A high health risk from COPD** attributable to ozone pollution (histSST) is found in South Asia and East Asia with a regional average AF of 13% and 12%, 470 respectively; while values in other regions are: **Ozone pollution in histSST is responsible for more than 10% of COPD deaths in South and East Asia; while percentages in other regions are:** North Africa and Middle East (9%), High-income Asia Pacific (9%), Central Europe (7%), Western Europe (6%) and High-income North America (5%). **Regarding the drivers of ozone**

changes, fixing NO_x emissions to pre-industrial levels (histSST-piNO_x) eliminates the risk for human health from ozone exposure for the 2005-2014 period in most regions. As for the drivers of ozone health effects, NO_x emissions in the historical period 475 are found to be the main contributor to ozone-related mortality for the 2005-2014 period, as fixing them to pre-industrial levels (histSST-piNO_x) eliminates the risk for human health from ozone exposure in the majority of regions. Historical increases in methane concentrations also appear to imply a risk for human health in near present-day both globally and regionally, as setting methane concentrations to pre-industrial levels results in a lower risk for health in the highly populated regions of South Asia, East Asia, and Western Europe with AF values of 9%, 7%, and 2%, respectively. Historical increases in methane 480 concentrations also appear to be a significant contributor to near present-day AF both globally and regionally. Setting methane concentrations to pre-industrial levels reduces ozone-related mortality in the highly populated regions of South Asia, East Asia and Western Europe by $\approx 4\%$ and that of High-income North America by $\approx 3\%$. Historical changes in climate, aerosol precursor emissions and stratospheric ozone have relatively small impacts on historical OSDMA8 changes and consequently on regional mean near present-day AF. regional mean near present-day AF. Isolating these drivers at 1850 levels (or 1950 for stratospheric 485 ozone) shows only small changes in AF values and therefore in ozone-related health risk. a small ($\approx 1\%$) increase in the risk to ozone-related mortality.

4 Conclusions

Surface ozone is an important greenhouse gas and secondary pollutant in the lower atmosphere, influencing both the Earth's climate and air quality. Exposure to elevated concentrations of ozone at the surface can have detrimental impacts on human health. 490 In this work we use numerical results of hourly surface ozone, obtained from the latest generation of global chemistry climate models that participated in CMIP6, as part of the Aerosol and Chemistry Model Intercomparison Project (AerChemMIP). For the first time we use hourly surface ozone output from three different CMIP6 models, over the 165-year historical period (1850 to 2014), to calculate changes in the peak season ozone metric (OSDMA8), that can relate risks to human health from long-term exposure surface ozone. All three CMIP6 models tended to overestimate the recent observed OSDMA8 concentrations, in agreement with other recent multi-model evaluations of surface ozone concentrations (Young et al., 2018; Turnock 495 et al., 2020). The most recent 10-year mean period (2005 to 2014) of OSDMA8 concentrations simulated by the three CMIP6 models were bias-corrected to the observations to avoid overestimating the present-day risk to human health from long-term ozone exposure. However, there is still a 10 to 15% difference in the simulated OSDMA8 concentrations in the pre-industrial period (1850 to 1859) due to physical and chemical differences across the three models, which also influences the magnitude of 500 the simulated historical change in OSDMA8. Global increases of more than 50% in OSDMA8 concentrations were simulated over the historical period by all three CMIP6 models, with the largest changes over the Northern Hemisphere regions (North America, Europe, Asia). This change has increased the proportion of the global population being exposed to OSDMA8 concentrations above the theoretical minimum risk exposure level (TMREL), below which ozone is considered as not being harmful for human health, from less than 20% in 1855 to more than 90% in 2010. The risk to human health from long-term exposure to 505 ozone concentrations has been assessed in terms of changes to the attributable fraction (AF), defined here as the percentage of

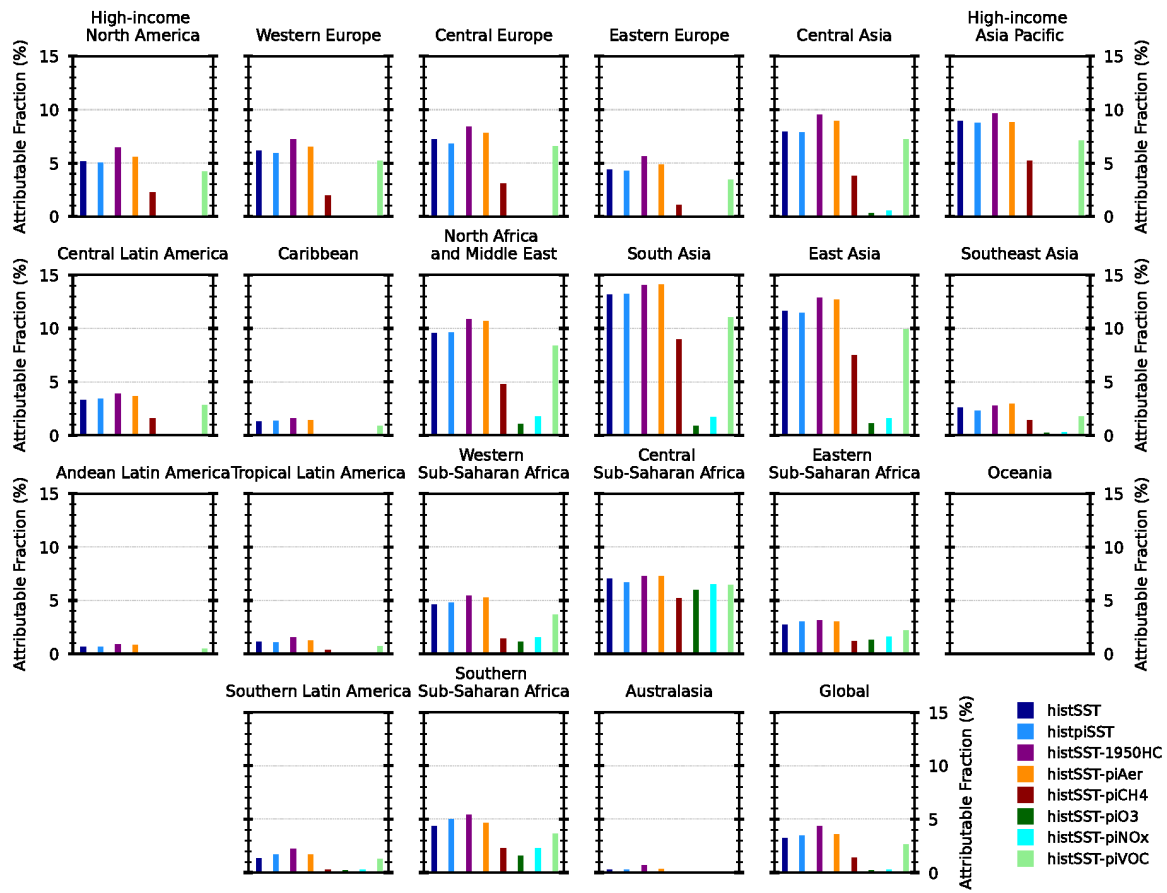


Figure 7. Regional mean attributable fraction as the percentage of deaths from COPD calculated from the 10 year (2005-14) mean OSDMA8 values simulated by UKESM1-0-LL in the HistSST and sensitivity experiments with different drivers of ozone fixed

deaths from chronic obstructive pulmonary disease (COPD) attributable to ozone pollution. The AF has increased by more than 10% over many regions of the Northern Hemisphere, showing that increased ozone concentrations over the historical period have contributed to a significant increase in the long-term risk to human health across many populated regions of the world. In addition, the historical increase in surface ozone concentrations has made the risk of human mortality from long-term exposure

510 to ozone similar to other environmental risk factors, but still much less than from long-term exposure to fine particulate matter (GBD 2021 Risk Factors Collaborators, 2024).

An analysis of the drivers of historical changes in OSDMA8 concentrations and risks to human health is provided from hourly surface ozone outputs of sensitivity experiments conducted using a single CMIP6 model that isolate the historical 515 changes in ozone precursors (NO_x , CO , non- CH_4 VOCs and CH_4), anthropogenic aerosols, ozone depleting substances and climate change. Historical increases in anthropogenic emissions of NO_x is identified as the leading contributor to increases

in OSDMA8 concentrations ($\approx 40\%$ globally) over the period 1850 to 2014, particularly over Northern Hemisphere regions. Increases in global CH₄ concentrations is also shown to have an important contribution to the historical changes in OSDMA8 concentrations ($\approx 30\%$ globally), particularly over more southern hemisphere regions where its contribution can be as large of 520 that from NO_x. The increase in anthropogenic emissions of other ozone precursors (CO and non-CH₄ VOCs) has had a relatively small impact on increasing historical OSDMA8 concentrations ($\approx 7\%$ globally) compared to NO_x and CH₄. The other drivers considered here (stratospheric ozone, aerosols and climate change) all have relatively small contributions to historical 525 changes in OSDMA8 concentrations. The depletion of stratospheric ozone since the 1950s has resulted in less downward transport of ozone to the surface and a small reduction in historical surface concentrations, particularly over more remote Southern Hemisphere regions. Increasing anthropogenic emissions of aerosols also caused a small reduction in OSDMA8 530 concentrations, particularly over Asia, although this effect might be underestimated due an under representation of heterogeneous chemistry mechanisms within the model (Ivatt et al., 2022). Historical climate change contributed to a small reductions in historical OSDMA8 concentrations over remote regions and a small increase over polluted continental regions due to changes in ozone production and destruction pathways. The response of ozone to climate change was small due to the small 1K of 535 global warming considered over the historical period, although the results were consistent with projected changes due to future warming (Zanis et al., 2022).

Increasing anthropogenic NO_x emissions over the 1850 to 2014 period is shown to be the main contributor to the long-term 535 health effects from ozone exposure in the near present day period (2010). Fixing anthropogenic NO_x emissions at 1850 reduces the proportion of the near present day global population exposed to OSDMA8 concentrations above the TMREL to 34%, from more than 90% when they are allowed to increase over the historical period along with other precursors. Fixing NO_x emissions 540 at 1850 also reduces the AF to near zero across most regions, thereby eliminating the risk to human health from long-term ozone exposure. Historical global CH₄ concentrations are shown to be the next most important contributor to the health effects from long-term ozone exposure. Fixing global CH₄ concentrations at 1850 values reduces the proportion of the global population exposed to OSDMA8 concentrations above the TMREL to 83%, and reduces the AF, and risk to human health, by about half in populated regions. However, the influence of the other drivers is small, having little impact on the health risk of the near 545 present day population from exposure to elevated surface ozone concentrations.

The results from these experiments provide a unique opportunity to quantify the long term changes, and **attribution to 545 multiple drivers** behind the changes, of an ozone exposure metric relevant to health impacts **over a 165-year period from 1850 to 2014**. Substantial increases have occurred in surface ozone concentrations and the risk to human health from long-term exposure to these elevated concentrations over the historical period. These changes can be mainly attributed to changes in anthropogenic sources of ozone precursors such as NO_x and CH₄, with smaller contributions from CO and non-CH₄ VOCs. Sensitivity studies show that drastic changes to these main drivers can have large impacts on the risk to human health. However, 550 there are also non-negligible changes due to other drivers of ozone (stratospheric ozone, aerosols and climate change), which could become more significant in the future depending on the particular emissions and climate pathway the world takes.

Therefore, understanding the historical changes and drivers of ozone and human health could help to inform future policy measures.

Data availability. The hourly surface ozone data used in this study has been obtained from the CMIP6 data archive which is hosted at the Earth System Grid Federation and is freely available to download from <https://esgf-node.llnl.gov/search/cmip6/>. The references for AerChemMIP data used from GFDL-ESM4, EC-Earth3-AerChem and UKESM1-0-ll are Horowitz et al. (2018); EC-Earth Consortium (2020); O'Connor (2019). The CMIP6 variable name sfo3 has been used from the experiments listed in Table 1. Processed model data and calculations related to human health that are used in this study can be found on zenodo at <https://doi.org/10.5281/zenodo.13385648>. The RAMP surface ozone observational data is from Becker et al. (2023).

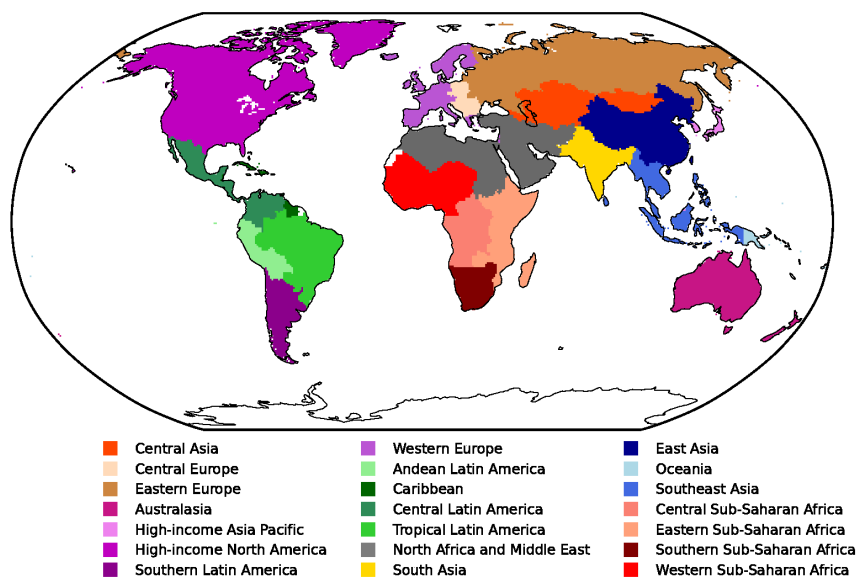


Figure A1. 21 regions used in this study based on those from the Global Burden of Disease study

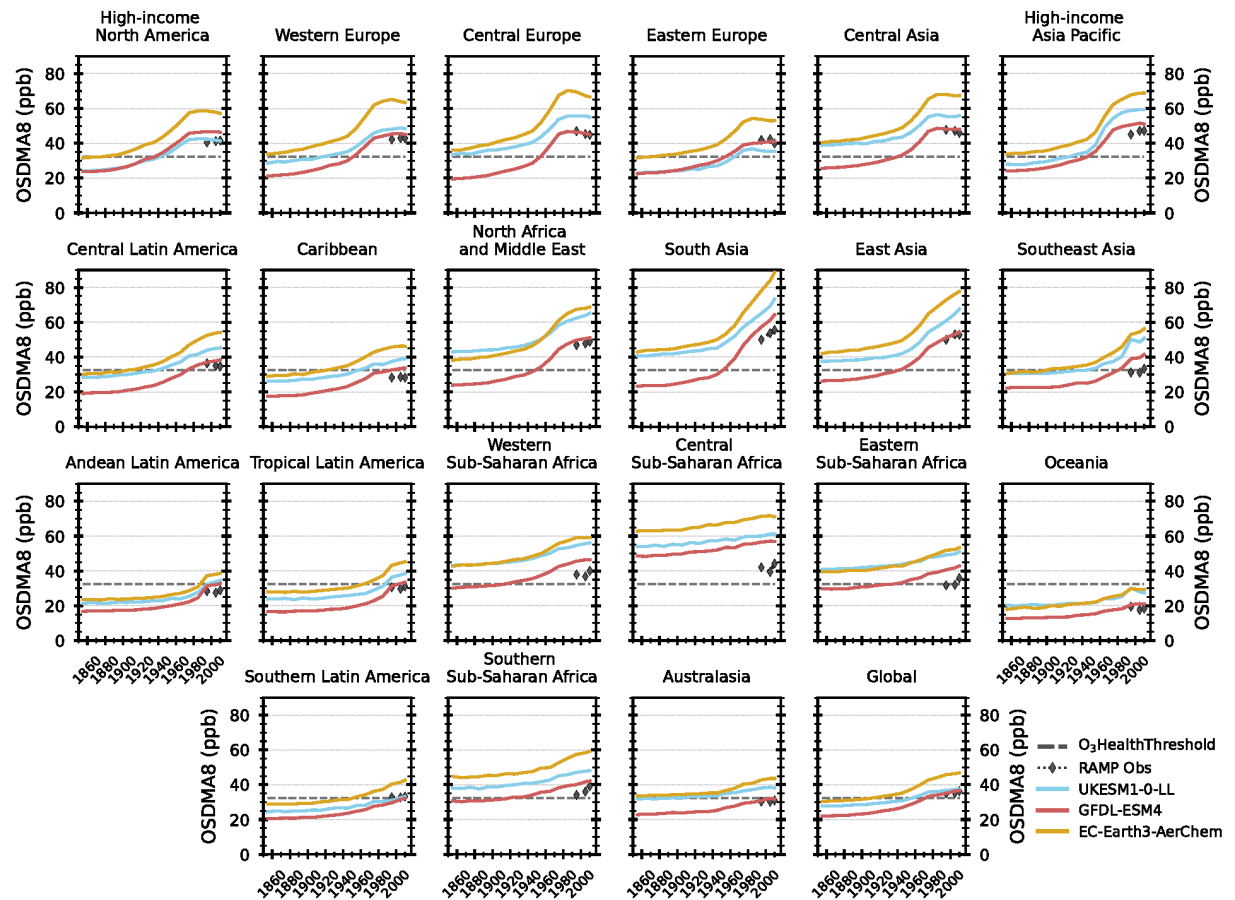


Figure A2. Uncorrected 10-year mean regional mean surface OSDMA8 values from 3 CMIP6 models simulated over the historical period (1850-2014) with 10-year mean values from RAMP observations (Becker et al., 2023) shown in grey diamonds.

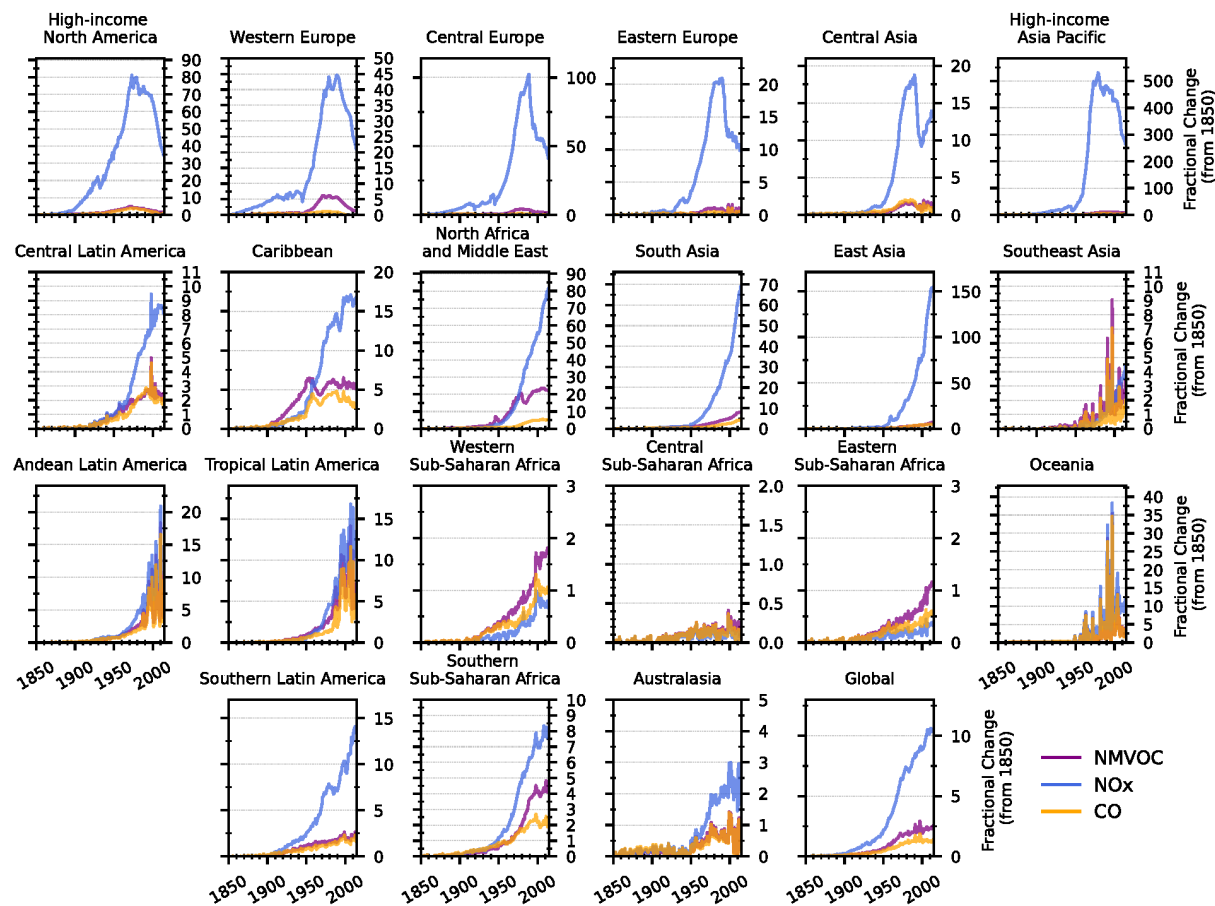


Figure A3. Relative change in historical regional emissions of ozone precursors (NOx, CO and non-CH₄ VOCs- NMVOCs) compared to 1850 values.

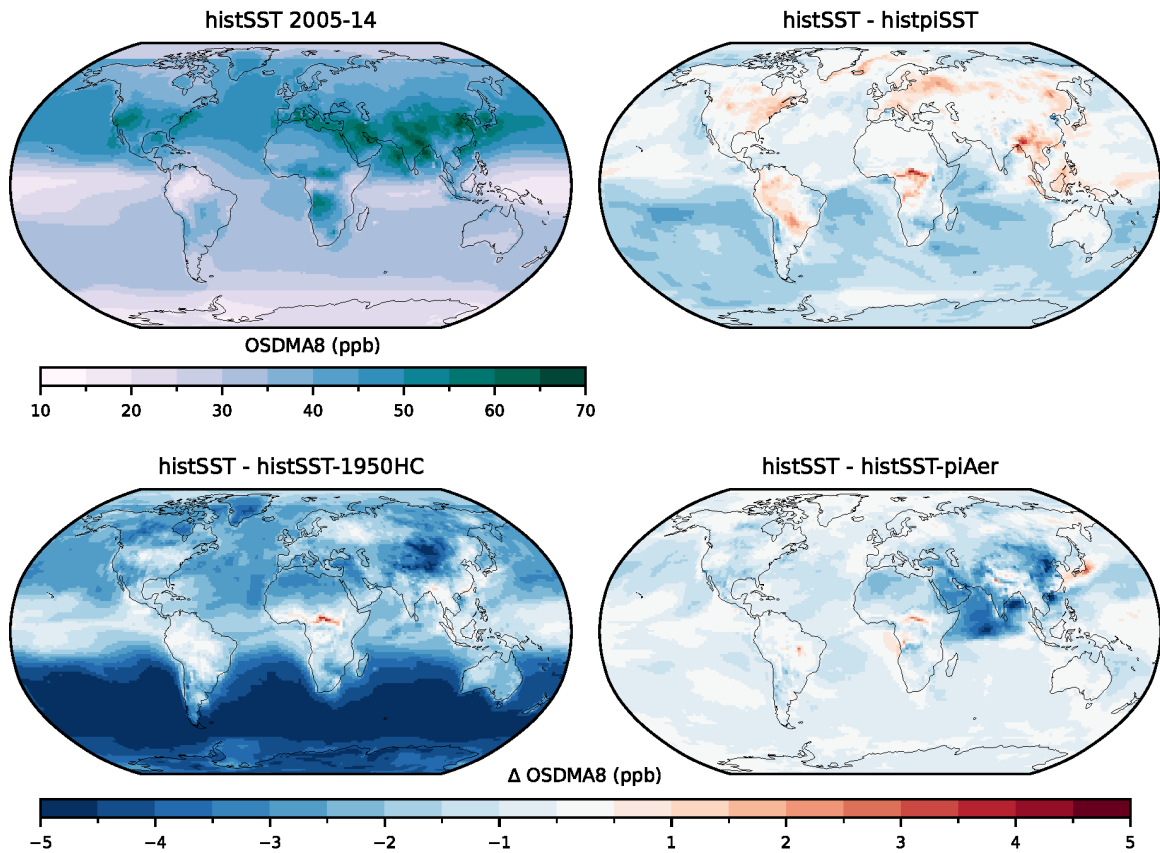


Figure A4. 10-year mean in surface OSDMA8 values simulated by UKESM1-0-LL in the HistSST experiment for 2005-14 (bias-corrected) and the change in the same time period in the HistSST experiment relative to the histpiSST, histSST-1950HC and histSST-piAer sensitivity experiments with different drivers of ozone (climate change, stratospheric ozone and aerosols) fixed. Same information as Figure 6 but different colour scale used

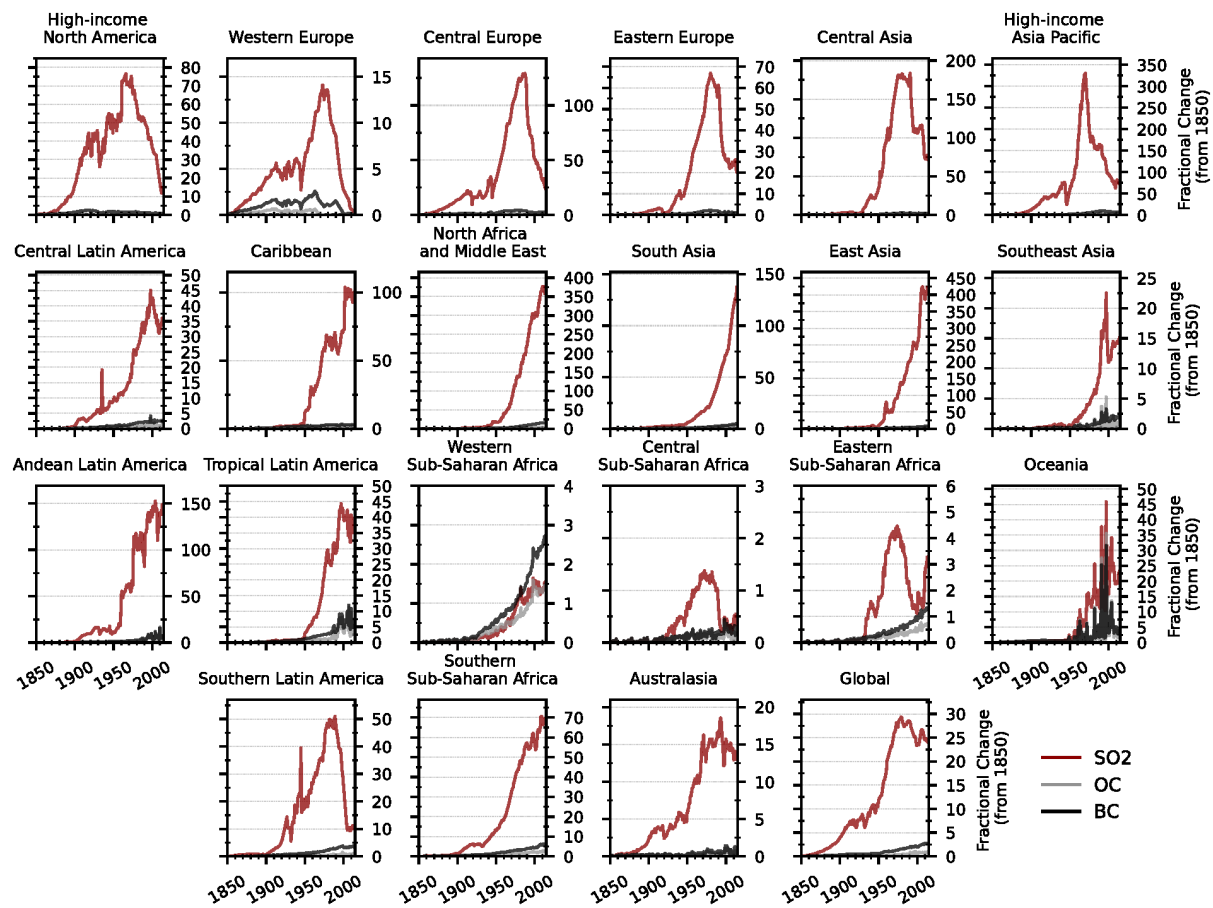


Figure A5. Relative change in historical regional emissions of ozone precursors (SO₂, OC and BC) compared to 1850 values

Table A1. Brief description of Aerosol and Chemistry relevant Processes in the models used in this study

Model	Resolution	Aerosol Scheme	Chemistry Scheme	Interactive Elements	Reference
EC-Earth3-AerChem	Approximately $3^{\circ} \times 2^{\circ}$ in horizontal (250km) and L34 (0.1hPa) in the vertical	M7 modal aerosol micro-physical scheme for SO_4 , BC, OA, sea salt, and mineral dust in 4 soluble and 3 insoluble modes. NH_4 , NO_3 , MSA using Equilibrium Simplified Aerosol Model (EQSAM).	TM5 chemistry scheme accounts for gas-phase, aqueous-phase, and heterogeneous chemistry based on modified version of the CB05 carbon bond mechanism.	Biogenic emissions of VOCs and CO are prescribed using monthly estimates from the MEGAN-MACC data set for the year 2000. Online emissions of mineral dust and sea salt, the oceanic source of DMS, and the production of nitrogen oxides (NO_x) by lightning. terrestrial DMS emissions from soils and vegetation, biogenic emissions of NO_x and NH_3 from soils, oceanic emissions of CO, NMVOCs and NH_3 , and SO_2 fluxes from continuously emitting volcanoes.	(van Noije et al., 2021)
GFDL-ESM4	Cubed-sphere (c96) grid, with ≈ 100 km native resolution, regridded to $1.0^{\circ} \times 1.25^{\circ}$ and L49 (0.01 hPa) in vertical	Bulk mass-based scheme for NH_4 , SO_4 , NO_3 , BC, OM, sea salt and dust. 5 size bins are used for sea salt and dust.	Interactive stratosphere-troposphere. 43 photolysis reactions, 190 gas-phase kinetic reactions and 15 heterogeneous reactions. NO_x - HO_x - O_x -chemical cycles and CO, CH_4 and NMVOC oxidation reactions.	DMS and sea salt emissions calculated online as a function of wind speed (and a prescribed DMS seawater climatology). Dust emissions coupled to interactive vegetation. Lightning NO_x calculated online as a function of convection. Online emissions of BVOCs (isoprene and monoterpenes) calculated from a prescribed vegetation cover using MEGAN2.1 algorithm, which has dependence on light and temperature but also inhibits isoprene emissions based on CO_2 .	(Horowitz et al., 2020; Dunne et al., 2020)
UKESM1-0-LL	$1.25^{\circ} \times 1.875^{\circ}$ in horizontal (150km) L85 (85km) in vertical	GLOMAP-Mode. (Modal scheme, mass and number) for SO_4 , BC, OM, sea salt. Mass based bin scheme used for mineral dust.	UKCA coupled stratosphere-troposphere. Interactive photolysis. 84 chemical tracers. Simulates chemical cycles of O_x , HO_x and NO_x , as well as oxidation reactions of CO, CH_4 and NMVOCs. In addition, heterogeneous processes, Cl and Br chemistry are included.	Online emissions of DMS, sea-salt and dust aerosols, as well as emissions of primary marine organics and biogenic organic compounds. Online NO_x calculated from lightning, Interactive emissions of Isoprene (linked to chemistry) and monoterpenes (linked to secondary aerosols) using light and temperature, but isoprene emissions are inhibited based on CO_2 .	(Archibald et al., 2020b; Mulcahy et al., 2020)

Author contributions. Steven T. Turnock set out the conceptual idea of the research project with inputs from Dimitris Akritidis and Andrea Pozzer. The main formal analysis, including the creation of figures, was conducted by Steven T. Turnock and Dimitris Akritidis. Observational data and additional analysis on this data was provided by Hantao Wang. Additional model data was provided by Larry Horowitz and Putian Zhou. Steven T. Turnock prepared the manuscript with contributions of writing and editing from all co-authors.

565 *Competing interests.* At least one of the (co-)authors is a member of the editorial board of Atmospheric Chemistry and Physics.

Acknowledgements. The contributions of Steven Turnock were funded by the Met Office Climate Science for Service Partnership (CSSP) China project under the International Science Partnerships Fund (ISPF). The contributions from Mariano Mertens were funded by the German Federal Ministry of Education and Research (Funding Nr.: 01LN2207A, IMPAC²T).

References

570 Akritidis, D., Pozzer, A., Flemming, J., Inness, A., and Zanis, P.: A Global Climatology of Tropopause Folds in CAMS and MERRA-2 Re-analyses, *Journal of Geophysical Research: Atmospheres*, 126, e2020JD034115, <https://doi.org/https://doi.org/10.1029/2020JD034115>, e2020JD034115 2020JD034115, 2021.

575 Akritidis, D., Bacer, S., Zanis, P., Georgoulias, A. K., Chowdhury, S., Horowitz, L. W., Naik, V., O'Connor, F. M., Keeble, J., Sager, P. L., van Noije, T., Zhou, P., Turnock, S., West, J. J., Lelieveld, J., and Pozzer, A.: Strong increase in mortality attributable to ozone pollution under a climate change and demographic scenario, *Environmental Research Letters*, 19, 024041, <https://doi.org/10.1088/1748-9326/ad2162>, 2024.

Anenberg, S. C., Horowitz, L. W., Tong, D. Q., and West, J. J.: An Estimate of the Global Burden of Anthropogenic Ozone and Fine Particulate Matter on Premature Human Mortality Using Atmospheric Modeling, *Environmental Health Perspectives*, 118, 1189–1195, <https://doi.org/10.1289/ehp.0901220>, 2010.

580 Archibald, A. T., Neu, J. L., Elshorbany, Y. F., Cooper, O. R., Young, P. J., Akiyoshi, H., Cox, R. A., Coyle, M., Derwent, R. G., Deushi, M., Finco, A., Frost, G. J., Galbally, I. E., Gerosa, G., Granier, C., Griffiths, P. T., Hossaini, R., Hu, L., Jöckel, P., Josse, B., Lin, M. Y., Mertens, M., Morgenstern, O., Naja, M., Naik, V., Oltmans, S., Plummer, D. A., Revell, L. E., Saiz-Lopez, A., Saxena, P., Shin, Y. M., Shahid, I., Shalercross, D., Tilmes, S., Trickl, T., Wallington, T. J., Wang, T., Worden, H. M., and Zeng, G.: Tropospheric Ozone Assessment Report: A critical review of changes in the tropospheric ozone burden and budget from 1850 to 2100, *Elementa: Science of the Anthropocene*, 8, 034, <https://doi.org/10.1525/elementa.2020.034>, 2020a.

585 Archibald, A. T., O'Connor, F. M., Abraham, N. L., Archer-Nicholls, S., Chipperfield, M. P., Dalvi, M., Folberth, G. A., Dennison, F., Dhomse, S. S., Griffiths, P. T., Hardacre, C., Hewitt, A. J., Hill, R. S., Johnson, C. E., Keeble, J., Köhler, M. O., Morgenstern, O., Mulcahy, J. P., Ordóñez, C., Pope, R. J., Rumbold, S. T., Russo, M. R., Savage, N. H., Sellar, A., Stringer, M., Turnock, S. T., Wild, O., and Zeng, G.: Description and evaluation of the UKCA stratosphere–troposphere chemistry scheme (StratTrop vn 1.0) implemented in UKESM1, *Geoscientific Model Development*, 13, 1223–1266, <https://doi.org/10.5194/gmd-13-1223-2020>, 2020b.

590 Archibald, A. T., Turnock, S. T., Griffiths, P. T., Cox, T., Derwent, R. G., Knote, C., and Shin, M.: On the changes in surface ozone over the twenty-first century: sensitivity to changes in surface temperature and chemical mechanisms, *Philosophical Transactions of the Royal Society A: Mathematical, Physical and Engineering Sciences*, 378, 20190329, <https://doi.org/10.1098/rsta.2019.0329>, 2020c.

595 Becker, J. S., DeLang, M. N., Chang, K.-L., Serre, M. L., Cooper, O. R., Wang, H., Schultz, M. G., Schröder, S., Lu, X., Zhang, L., Deushi, M., Josse, B., Keller, C. A., Lamarque, J.-F., Lin, M., Liu, J., Marécal, V., Strode, S. A., Sudo, K., Tilmes, S., Zhang, L., Brauer, M., and West, J. J.: Using Regionalized Air Quality Model Performance and Bayesian Maximum Entropy data fusion to map global surface ozone concentration, *Elementa: Science of the Anthropocene*, 11, 00025, <https://doi.org/10.1525/elementa.2022.00025>, 2023.

600 Chen, D., Rojas, M., Samset, B., Cobb, K., Diongue Niang, A., Edwards, P., Emori, S., Faria, S., Hawkins, E., Hope, P., Huybrechts, P., Meinshausen, M., Mustafa, S., Plattner, G.-K., and Tréguier, A.-M.: *Framing, Context, and Methods in Climate Change 2021: The Physical Science Basis: Working Group I Contribution to the Sixth Assessment Report of the Intergovernmental Panel on Climate Change*, p. 147–286, Cambridge University Press, <https://doi.org/10.1017/9781009157896.003>, 2021.

Chen, Z., Liu, J., Qie, X., Cheng, X., Yang, M., Shu, L., and Zang, Z.: Stratospheric influence on surface ozone pollution in China, *Nature Communications*, 15, <https://doi.org/10.1038/s41467-024-48406-x>, 2024.

Cohen, A. J., Anderson, H. R., Ostro, B., Pandey, K. D., Krzyzanowski, M., Künzli, N., Gutschmidt, K., Pope, A., Romieu, I., Samet, J. M.,
605 and Smith, K.: The Global Burden of Disease Due to Outdoor Air Pollution, *Journal of Toxicology and Environmental Health, Part A*, 68,
1301–1307, <https://doi.org/10.1080/15287390590936166>, pMID: 16024504, 2005.

Cohen, A. J., Brauer, M., Burnett, R., Anderson, H. R., Frostad, J., Estep, K., Balakrishnan, K., Brunekreef, B., Dandona, L., Dandona, R.,
Feigin, V., Freedman, G., Hubbell, B., Jobling, A., Kan, H., Knibbs, L., Liu, Y., Martin, R., Morawska, L., Pope, C. A., Shin, H., Straif,
K., Shaddick, G., Thomas, M., van Dingenen, R., van Donkelaar, A., Vos, T., Murray, C. J. L., and Forouzanfar, M. H.: Estimates and
610 25-year trends of the global burden of disease attributable to ambient air pollution: an analysis of data from the Global Burden of Diseases
Study 2015, *The Lancet*, 389, 1907–1918, [https://doi.org/https://doi.org/10.1016/S0140-6736\(17\)30505-6](https://doi.org/10.1016/S0140-6736(17)30505-6), 2017.

Collins, W. J., Lamarque, J.-F., Schulz, M., Boucher, O., Eyring, V., Hegglin, M. I., Maycock, A., Myhre, G., Prather, M., Shindell, D., and
Smith, S. J.: AerChemMIP: quantifying the effects of chemistry and aerosols in CMIP6, *Geoscientific Model Development*, 10, 585–607,
615 <https://doi.org/10.5194/gmd-10-585-2017>, 2017.

Dahlmann, K., Grewe, V., Ponater, M., and Matthes, S.: Quantifying the contributions of individual NO_x sources to the trend in ozone
radiative forcing, *Atmos. Environ.*, 45, 2860–2868, <https://doi.org/http://dx.doi.org/10.1016/j.atmosenv.2011.02.071>, 2011.

DeLang, M. N., Becker, J. S., Chang, K.-L., Serre, M. L., Cooper, O. R., Schultz, M. G., Schröder, S., Lu, X., Zhang, L., Deushi,
M., Josse, B., Keller, C. A., Lamarque, J.-F., Lin, M., Liu, J., Marécal, V., Strode, S. A., Sudo, K., Tilmes, S., Zhang, L., Cleland,
620 S. E., Collins, E. L., Brauer, M., and West, J. J.: Mapping Yearly Fine Resolution Global Surface Ozone through the Bayesian Maximum
Entropy Data Fusion of Observations and Model Output for 1990–2017, *Environmental Science & Technology*, 55, 4389–4398,
<https://doi.org/10.1021/acs.est.0c07742>, pMID: 33682412, 2021.

Doherty, R. M., Wild, O., Shindell, D. T., Zeng, G., MacKenzie, I. A., Collins, W. J., Fiore, A. M., Stevenson, D. S., Dentener, F. J., Schultz,
M. G., Hess, P., Derwent, R. G., and Keating, T. J.: Impacts of climate change on surface ozone and intercontinental ozone pollution: A
multi-model study, *Journal of Geophysical Research: Atmospheres*, 118, 3744–3763, <https://doi.org/10.1002/jgrd.50266>, 2013.

625 Dunne, J. P., Horowitz, L. W., Adcroft, A. J., Ginoux, P., Held, I. M., John, J. G., Krasting, J. P., Malyshev, S., Naik, V., Paulot, F., Shevliakova,
E., Stock, C. A., Zadeh, N., Balaji, V., Blanton, C., Dunne, K. A., Dupuis, C., Durachta, J., Dussin, R., Gauthier, P. P. G., Griffies, S. M.,
Guo, H., Hallberg, R. W., Harrison, M., He, J., Hurlin, W., McHugh, C., Menzel, R., Milly, P. C. D., Nikonorov, S., Paynter, D. J., Poshay,
J., Radhakrishnan, A., Rand, K., Reichl, B. G., Robinson, T., Schwarzkopf, D. M., Sentman, L. T., Underwood, S., Vahlenkamp, H.,
Winton, M., Wittenberg, A. T., Wyman, B., Zeng, Y., and Zhao, M.: The GFDL Earth System Model version 4.1 (GFDL-ESM 4.1):
630 Overall coupled model description and simulation characteristics, *Journal of Advances in Modeling Earth Systems*, p. 2019ms002015,
<https://doi.org/10.1029/2019ms002015>, 2020.

EC-Earth Consortium, E.-E.: EC-Earth-Consortium EC-Earth3-AerChem model output prepared for CMIP6 AerChemMIP,
<https://doi.org/10.22033/ESGF/CMIP6.699>, 2020.

EMEP Steering Body and Working Group on Effects of the Convention on Long-Range Transboundary Air Pollution: Towards Cleaner Air.
635 Scientific Assessment Report 2016., https://unece.org/sites/default/files/2021-06/CLRTAP_Scientific_Assessment_Report_en.pdf, 2016.

Fang, Y., Naik, V., Horowitz, L. W., and Mauzerall, D. L.: Air pollution and associated human mortality: the role of air pollutant emissions,
climate change and methane concentration increases from the preindustrial period to present, *Atmospheric Chemistry and Physics*, 13,
1377–1394, <https://doi.org/10.5194/acp-13-1377-2013>, 2013.

Fiore, A. M., Dentener, F. J., Wild, O., Cuvelier, C., Schultz, M. G., Hess, P., Textor, C., Schulz, M., Doherty, R. M., Horowitz, L. W.,
640 MacKenzie, I. A., Sanderson, M. G., Shindell, D. T., Stevenson, D. S., Szopa, S., Van Dingenen, R., Zeng, G., Atherton, C., Bergmann,
D., Bey, I., Carmichael, G., Collins, W. J., Duncan, B. N., Faluvegi, G., Folberth, G., Gauss, M., Gong, S., Hauglustaine, D., Hol-

loway, T., Isaksen, I. S. A., Jacob, D. J., Jonson, J. E., Kaminski, J. W., Keating, T. J., Lupu, A., Marmer, E., Montanaro, V., Park, R. J., Pitari, G., Pringle, K. J., Pyle, J. A., Schroeder, S., Vivanco, M. G., Wind, P., Wojcik, G., Wu, S., and Zuber, A.: Multimodel estimates of intercontinental source-receptor relationships for ozone pollution, *Journal of Geophysical Research: Atmospheres*, 114, 645 <https://doi.org/https://doi.org/10.1029/2008JD010816>, 2009.

Fleming, Z. L., Doherty, R. M., von Schneidemesser, E., Malley, C. S., Cooper, O. R., Pinto, J. P., Colette, A., Xu, X., Simpson, D., Schultz, M. G., Lefohn, A. S., Hamad, S., Moolla, R., Solberg, S., and Feng, Z.: Tropospheric Ozone Assessment Report: Present-day ozone distribution and trends relevant to human health, *Elementa: Science of the Anthropocene*, 6, 12, 650 <https://doi.org/10.1525/elementa.273>, 2018.

Flynn, C. M. and Mauritsen, T.: On the climate sensitivity and historical warming evolution in recent coupled model ensembles, *Atmospheric Chemistry and Physics*, 20, 7829–7842, <https://doi.org/10.5194/acp-20-7829-2020>, 2020.

Folberth, G. A., Staniaszek, Z., Archibald, A. T., Gedney, N., Griffiths, P. T., Jones, C. D., O'Connor, F. M., Parker, R. J., Sellar, A. A., and Wiltshire, A.: Description and Evaluation of an Emission-Driven and Fully Coupled Methane Cycle in UKESM1, *Journal of Advances in Modeling Earth Systems*, 14, e2021MS002982, 655 <https://doi.org/https://doi.org/10.1029/2021MS002982>, e2021MS002982 2021MS002982, 2022.

Forouzanfar, M., Alexander, L., Anderson, H., Bachman, V., Biryukov, S., Brauer, M., Burnett, R., Casey, D., Coates, M., Cohen, A., Delwiche, K., Estep, K., Frostad, J., Astha, K., Kyu, H., Moradi-Lakeh, M., Ng, M., Slepak, E., Thomas, B., Wagner, J., Aasvang, G., Abbafati, C., Ozgoren, A., Abd-Allah, F., Abera, S., Aboyans, V., Abraham, B., Abraham, J., Abubakar, I., Abu-Rmeileh, N., Aburto, T., Achoki, T., Adelekan, A., Adofo, K., Adou, A., Adsuar, J., Afshin, A., Agardh, E., Al Khabour, M., Al Lami, F., Alam, S., Alasfoor, D., 660 Amini, H., Brooks, P., Havmøller, R., Iburg, K., Juel, K., Larsson, A., Narayan, K., Zhao, Y., and GBD 2013 Risk Factors Collaborators: Global, regional, and national comparative risk assessment of 79 behavioural, environmental and occupational, and metabolic risks or clusters of risks in 188 countries, 1990-2013: a systematic analysis for the Global Burden of Disease Study 2013, *The Lancet*, 386, 2287–2323, [https://doi.org/10.1016/S0140-6736\(15\)00128-2](https://doi.org/10.1016/S0140-6736(15)00128-2), 2015.

Fortems-Cheiney, A., Foret, G., Siour, G., Vautard, R., Szopa, S., Dufour, G., Colette, A., Lacressonniere, G., and Beekmann, M.: A 3 665 °C global RCP8.5 emission trajectory cancels benefits of European emission reductions on air quality, *Nature Communications*, 8, 1–5, <https://doi.org/10.1038/s41467-017-00075-9>, 2017.

Fu, T.-M. and Tian, H.: Climate Change Penalty to Ozone Air Quality: Review of Current Understandings and Knowledge Gaps, *Current Pollution Reports*, 5, 159–171, <https://doi.org/10.1007/s40726-019-00115-6>, 2019.

Gao, Y., Zhang, J., Yan, F., Leung, L. R., Luo, K., Zhang, Y., and Bell, M. L.: Nonlinear effect of compound extreme weather events on ozone 670 formation over the United States, *Weather and Climate Extremes*, 30, 100 285, <https://doi.org/https://doi.org/10.1016/j.wace.2020.100285>, 2020.

GBD 2021 Risk Factors Collaborators: Global burden and strength of evidence for 88 risk factors in 204 countries and 811 sub-national locations, 1990-2021: a systematic analysis for the Global Burden of Disease Study 2021, *The Lancet*, 403, 2162–2203, 675 [https://doi.org/https://doi.org/10.1016/S0140-6736\(24\)00933-4](https://doi.org/https://doi.org/10.1016/S0140-6736(24)00933-4), 2024.

Griffiths, P. T., Murray, L. T., Zeng, G., Shin, Y. M., Abraham, N. L., Archibald, A. T., Deushi, M., Emmons, L. K., Galbally, I. E., Hassler, B., Horowitz, L. W., Keeble, J., Liu, J., Moeini, O., Naik, V., O'Connor, F. M., Oshima, N., Tarasick, D., Tilmes, S., Turnock, S. T., Wild, O., Young, P. J., and Zanis, P.: Tropospheric ozone in CMIP6 simulations, *Atmospheric Chemistry and Physics*, 21, 4187–4218, 680 <https://doi.org/10.5194/acp-21-4187-2021>, 2021.

680 Hoesly, R. M., Smith, S. J., Feng, L., Klimont, Z., Janssens-Maenhout, G., Pitkanen, T., Seibert, J. J., Vu, L., Andres, R. J., Bolt, R. M., Bond, T. C., Dawidowski, L., Kholod, N., Kurokawa, J.-I., Li, M., Liu, L., Lu, Z., Moura, M. C. P., O'Rourke, P. R., and Zhang, Q.: Historical (1750–2014) anthropogenic emissions of reactive gases and aerosols from the Community Emissions Data System (CEDS), *Geoscientific Model Development*, 11, 369–408, <https://doi.org/10.5194/gmd-11-369-2018>, 2018.

685 Horowitz, L. W., Naik, V., Sentman, L., Paulot, F., Blanton, C., McHugh, C., Radhakrishnan, A., Rand, K., Vahlenkamp, H., Zadeh, N. T., Wilson, C., Ginoux, P., He, J., John, J. G., Lin, M., Paynter, D. J., Ploshay, J., Zhang, A., and Zeng, Y.: NOAA-GFDL GFDL-ESM4 model output prepared for CMIP6 AerChemMIP, <https://doi.org/10.22033/ESGF/CMIP6.1404>, 2018.

690 Horowitz, L. W., Naik, V., Paulot, F., Ginoux, P. A., Dunne, J. P., Mao, J., Schnell, J., Chen, X., He, J., John, J. G., Lin, M., Lin, P., Malyshev, S., Paynter, D., Shevliakova, E., and Zhao, M.: The GFDL Global Atmospheric Chemistry-Climate Model AM4.1: Model Description and Simulation Characteristics, *Journal of Advances in Modeling Earth Systems*, 12, e2019MS002032, <https://doi.org/https://doi.org/10.1029/2019MS002032>, 2019MS002032, 2020.

695 Iglesias-Suarez, F., Kinnison, D. E., Rap, A., Maycock, A. C., Wild, O., and Young, P. J.: Key drivers of ozone change and its radiative forcing over the 21st century, *Atmospheric Chemistry and Physics*, 18, 6121–6139, <https://doi.org/10.5194/acp-18-6121-2018>, 2018.

700 Ivatt, P. D., Evans, M. J., and Lewis, A. C.: Suppression of surface ozone by an aerosol-inhibited photochemical ozone regime, *Nature Geoscience* 2022 15:7, 15, 536–540, <https://doi.org/10.1038/s41561-022-00972-9>, 2022.

705 Johnson, C. E., Collins, W. J., Stevenson, D. S., and Derwent, R. G.: Relative roles of climate and emissions changes on future tropospheric oxidant concentrations, *Journal of Geophysical Research Atmospheres*, 104, 18 631–18 645, <https://doi.org/10.1029/1999JD900204>, 1999.

710 Keeble, J., Hassler, B., Banerjee, A., Checa-Garcia, R., Chiodo, G., Davis, S., Eyring, V., Griffiths, P. T., Morgenstern, O., Nowack, P., Zeng, G., Zhang, J., Bodeker, G., Burrows, S., Cameron-Smith, P., Cugnet, D., Danek, C., Deushi, M., Horowitz, L. W., Kubin, A., Li, L., Lohmann, G., Michou, M., Mills, M. J., Nabat, P., Olivié, D., Park, S., Seland, Ø., Stoll, J., Wieners, K.-H., and Wu, T.: Evaluating stratospheric ozone and water vapour changes in CMIP6 models from 1850 to 2100, *Atmospheric Chemistry and Physics*, 21, 5015–5061, <https://doi.org/10.5194/acp-21-5015-2021>, 2021.

715 Klein Goldewijk, K., Beusen, A., Doelman, J., and Stehfest, E.: Anthropogenic land use estimates for the Holocene – HYDE 3.2, *Earth System Science Data*, 9, 927–953, <https://doi.org/10.5194/essd-9-927-2017>, 2017.

720 Lelieveld, J. and Dentener, F. J.: What controls tropospheric ozone?, *Journal of Geophysical Research: Atmospheres*, 105, 3531–3551, <https://doi.org/https://doi.org/10.1029/1999JD901011>, 2000.

725 Lelieveld, J., Evans, J. S., Fnais, M., Giannadaki, D., and Pozzer, A.: The contribution of outdoor air pollution sources to premature mortality on a global scale, *Nature*, 525, 367–371, <https://doi.org/10.1038/nature15371>, 2015.

730 Lelieveld, J., Pozzer, A., Pöschl, U., Fnais, M., Haines, A., and Münzel, T.: Loss of life expectancy from air pollution compared to other risk factors: a worldwide perspective, *Cardiovascular Research*, 116, 1910–1917, <https://doi.org/10.1093/cvr/cvaa025>, 2020.

735 Liang, C.-K., West, J. J., Silva, R. A., Bian, H., Chin, M., Davila, Y., Dentener, F. J., Emmons, L., Flemming, J., Folberth, G., Henze, D., Im, U., Jonson, J. E., Keating, T. J., Kucsera, T., Lenzen, A., Lin, M., Lund, M. T., Pan, X., Park, R. J., Pierce, R. B., Sekiya, T., Sudo, K., and Takemura, T.: HTAP2 multi-model estimates of premature human mortality due to intercontinental transport of air pollution and emission sectors, *Atmospheric Chemistry and Physics*, 18, 10 497–10 520, <https://doi.org/10.5194/acp-18-10497-2018>, 2018.

740 Lim, S. S., Vos, T., Flaxman, A. D., Danaei, G., Shibuya, K., Adair-Rohani, H., AlMazroa, M. A., Amann, M., Anderson, H. R., Andrews, K. G., et al.: A comparative risk assessment of burden of disease and injury attributable to 67 risk factors and risk factor clusters in 21 regions, 1990–2010: a systematic analysis for the Global Burden of Disease Study 2010, *The lancet*, 380, 2224–2260, [https://doi.org/https://doi.org/10.1016/S0140-6736\(12\)61766-8](https://doi.org/https://doi.org/10.1016/S0140-6736(12)61766-8), 2012.

Lin, M., Horowitz, L. W., Payton, R., Fiore, A. M., and Tonnesen, G.: US surface ozone trends and extremes from 1980 to 2014: quantifying the roles of rising Asian emissions, domestic controls, wildfires, and climate, *Atmospheric Chemistry and Physics*, 17, 2943–2970, <https://doi.org/10.5194/acp-17-2943-2017>, 2017.

720 720 Malashock, D. A., DeLang, M. N., Becker, J. S., Serre, M. L., West, J. J., Chang, K.-L., Cooper, O. R., and Anenberg, S. C.: Estimates of ozone concentrations and attributable mortality in urban, peri-urban and rural areas worldwide in 2019, *Environmental Research Letters*, 17, 054 023, <https://doi.org/10.1088/1748-9326/ac66f3>, 2022.

725 Malley, C. S., Henze, D. K., Kuylenstierna, J. C., Vallack, H. W., Davila, Y., Anenberg, S. C., Turner, M. C., and Ashmore, M. R.: Updated global estimates of respiratory mortality in adults ≥ 30 years of age attributable to long-term ozone exposure, *Environmental health perspectives*, 125, 087 021, <https://doi.org/10.1289/EHP1390>, 2017.

Mertens, M., Brinkop, S., Graf, P., Grewe, V., Hendricks, J., Jöckel, P., Lanteri, A., Matthes, S., Rieger, V. S., Righi, M., and Thor, R. N.: The contribution of transport emissions to ozone mixing ratios and methane lifetime in 2015 and 2050 in the Shared Socioeconomic Pathways (SSPs), *EGUphere*, 2024, 1–45, <https://doi.org/10.5194/egusphere-2024-324>, 2024.

730 Mills, G., Pleijel, H., Malley, C. S., Sinha, B., Cooper, O. R., Schultz, M. G., Neufeld, H. S., Simpson, D., Sharps, K., Feng, Z., Gerosa, G., Harmens, H., Kobayashi, K., Saxena, P., Paoletti, E., Sinha, V., and Xu, X.: Tropospheric Ozone Assessment Report: Present-day tropospheric ozone distribution and trends relevant to vegetation, *Elementa: Science of the Anthropocene*, 6, 47, <https://doi.org/10.1525/elementa.302>, 2018.

735 Monks, P. S., Archibald, A. T., Colette, A., Cooper, O., Coyle, M., Derwent, R., Fowler, D., Granier, C., Law, K. S., Mills, G. E., Stevenson, D. S., Tarasova, O., Thouret, V., von Schneidemesser, E., Sommariva, R., Wild, O., and Williams, M. L.: Tropospheric ozone and its precursors from the urban to the global scale from air quality to short-lived climate forcer, *Atmospheric Chemistry and Physics*, 15, 8889–8973, <https://doi.org/10.5194/acp-15-8889-2015>, 2015.

740 Morgenstern, O., Stone, K. A., Schofield, R., Akiyoshi, H., Yamashita, Y., Kinnison, D. E., Garcia, R. R., Sudo, K., Plummer, D. A., Scinocca, J., Oman, L. D., Manyin, M. E., Zeng, G., Rozanov, E., Stenke, A., Revell, L. E., Pitari, G., Mancini, E., Di Genova, G., Visioni, D., Dhomse, S. S., and Chipperfield, M. P.: Ozone sensitivity to varying greenhouse gases and ozone-depleting substances in CCMI-1 simulations, *Atmospheric Chemistry and Physics*, 18, 1091–1114, <https://doi.org/10.5194/acp-18-1091-2018>, 2018.

Morice, C. P., Kennedy, J. J., Rayner, N. A., Winn, J. P., Hogan, E., Killick, R. E., Dunn, R. J. H., Osborn, T. J., Jones, P. D., and Simpson, I. R.: An Updated Assessment of Near-Surface Temperature Change From 1850: The HadCRUT5 Data Set, *Journal of Geophysical Research: Atmospheres*, 126, e2019JD032 361, <https://doi.org/10.1029/2019JD032361>, e2019JD032361 2019JD032361, 2021.

745 745 Mulcahy, J. P., Johnson, C., Jones, C. G., Povey, A. C., Scott, C. E., Sellar, A., Turnock, S. T., Woodhouse, M. T., Abraham, N. L., Andrews, M. B., Bellouin, N., Browse, J., Carslaw, K. S., Dalvi, M., Folberth, G. A., Glover, M., Grosvenor, D. P., Hardacre, C., Hill, R., Johnson, B., Jones, A., Kipling, Z., Mann, G., Molland, J., O'Connor, F. M., Palmiéri, J., Reddington, C., Rumbold, S. T., Richardson, M., Schutgens, N. A. J., Stier, P., Stringer, M., Tang, Y., Walton, J., Woodward, S., and Yool, A.: Description and evaluation of aerosol in UKESM1 and HadGEM3-GC3.1 CMIP6 historical simulations, *Geoscientific Model Development*, 13, 6383–6423, <https://doi.org/10.5194/gmd-13-6383-2020>, 2020.

Mulcahy, J. P., Jones, C. G., Rumbold, S. T., Kuhlbrodt, T., Dittus, A. J., Blockley, E. W., Yool, A., Walton, J., Hardacre, C., Andrews, T., Bodas-Salcedo, A., Stringer, M., de Mora, L., Harris, P., Hill, R., Kelley, D., Robertson, E., and Tang, Y.: UKESM1.1: development and evaluation of an updated configuration of the UK Earth System Model, *Geoscientific Model Development*, 16, 1569–1600, <https://doi.org/10.5194/gmd-16-1569-2023>, 2023.

755 Murray, C. J., Aravkin, A. Y., Zheng, P., Abbafati, C., Abbas, K. M., Abbasi-Kangevari, M., Abd-Allah, F., Abdelalim, A., Abdollahi, M., Abdollahpour, I., et al.: Global burden of 87 risk factors in 204 countries and territories, 1990–2019: a systematic analysis for the Global Burden of Disease Study 2019, *The lancet*, 396, 1223–1249, [https://doi.org/10.1016/S0140-6736\(20\)30752-2](https://doi.org/10.1016/S0140-6736(20)30752-2), 2020.

O'Connor, F.: MOHC UKESM1.0-LL model output prepared for CMIP6 AerChemMIP, <https://doi.org/10.22033/ESGF/CMIP6.1561>, 2019.

O'Connor, F. M., Abraham, N. L., Dalvi, M., Folberth, G. A., Griffiths, P. T., Hardacre, C., Johnson, B. T., Kahana, R., Keeble, J., Kim, B.,
760 Morgenstern, O., Mulcahy, J. P., Richardson, M., Robertson, E., Seo, J., Shim, S., Teixeira, J. C., Turnock, S. T., Williams, J., Wiltshire, A. J., Woodward, S., and Zeng, G.: Assessment of pre-industrial to present-day anthropogenic climate forcing in UKESM1, *Atmospheric Chemistry and Physics*, 21, 1211–1243, <https://doi.org/10.5194/acp-21-1211-2021>, 2021.

Ostro, B., Organization, W. H., et al.: Outdoor air pollution: assessing the environmental burden of disease at national and local levels, *World Health Organization*, 2004.

765 Parrish, D. D., Lamarque, J.-F., Naik, V., Horowitz, L., Shindell, D. T., Staehelin, J., Derwent, R., Cooper, O. R., Tanimoto, H., Volz-Thomas, A., Gilge, S., Scheel, H.-E., Steinbacher, M., and Fröhlich, M.: Long-term changes in lower tropospheric baseline ozone concentrations: Comparing chemistry-climate models and observations at northern midlatitudes, *Journal of Geophysical Research: Atmospheres*, 119, 5719–5736, [https://doi.org/https://doi.org/10.1002/2013JD021435](https://doi.org/10.1002/2013JD021435), 2014.

Parrish, D. D., Derwent, R. G., Turnock, S. T., O'Connor, F. M., Staehelin, J., Bauer, S. E., Deushi, M., Oshima, N., Tsigaridis, K., Wu,
770 T., and Zhang, J.: Investigations on the anthropogenic reversal of the natural ozone gradient between northern and southern midlatitudes, *Atmospheric Chemistry and Physics*, 21, 9669–9679, <https://doi.org/10.5194/acp-21-9669-2021>, 2021.

Pope, C. A., Burnett, R. T., Thun, M. J., Calle, E. E., Krewski, D., Ito, K., and Thurston, G. D.: Lung Cancer, Cardiopulmonary Mortality, and Long-term Exposure to Fine Particulate Air Pollution, *JAMA*, 287, 1132–1141, <https://doi.org/10.1001/jama.287.9.1132>, 2002.

Pozzer, A., Anenberg, S. C., Dey, S., Haines, A., Lelieveld, J., and Chowdhury, S.: Mortality Attributable to Ambient Air Pollution: A
775 Review of Global Estimates, *GeoHealth*, 7, e2022GH000711, <https://doi.org/https://doi.org/10.1029/2022GH000711>, e2022GH000711 2022GH000711, 2023.

Pozzer, A., Steffens, B., Proestos, Y., Sciare, J., Akritidis, D., Chowdhury, S., Burkart, K., and Bacer, S.: Atmospheric health burden across the century and the accelerating impact of temperature compared to pollution, *Nature Communications*, 15, 9379, <https://doi.org/10.1038/s41467-024-53649-9>, 2024.

780 Prather, M. J.: Time scales in atmospheric chemistry: Theory, GWPs for CH₄ and CO, and runaway growth, *Geophysical Research Letters*, 23, 2597–2600, <https://doi.org/https://doi.org/10.1029/96GL02371>, 1996.

Qu, Y., Voulgarakis, A., Wang, T., Kasoar, M., Wells, C., Yuan, C., Varma, S., and Mansfield, L.: A study of the effect of aerosols on surface ozone through meteorology feedbacks over China, *Atmospheric Chemistry and Physics*, 21, 5705–5718, <https://doi.org/10.5194/acp-21-5705-2021>, 2021.

785 Rowlinson, M. J., Rap, A., Hamilton, D. S., Pope, R. J., Hantson, S., Arnold, S. R., Kaplan, J. O., Arneth, A., Chipperfield, M. P., Forster, P. M., and Nieradzik, L.: Tropospheric ozone radiative forcing uncertainty due to pre-industrial fire and biogenic emissions, *Atmospheric Chemistry and Physics*, 20, 10937–10951, <https://doi.org/10.5194/acp-20-10937-2020>, 2020.

Schnell, J. L., Prather, M. J., Josse, B., Naik, V., Horowitz, L. W., Zeng, G., Shindell, D. T., and Faluvegi, G.: Effect of climate change on surface ozone over North America, Europe, and East Asia, *Geophysical Research Letters*, 43, 3509–3518,
790 <https://doi.org/https://doi.org/10.1002/2016GL068060>, 2016.

Sellar, A. A., Jones, C. G., Mulcahy, J., Tang, Y., Yool, A., Wiltshire, A., O'Connor, F. M., Stringer, M., Hill, R., Palmieri, J., Woodward, S., Mora, L., Kuhlbrodt, T., Rumbold, S., Kelley, D. I., Ellis, R., Johnson, C. E., Walton, J., Abraham, N. L., Andrews, M. B., Andrews,

795 T., Archibald, A. T., Berthou, S., Burke, E., Blockley, E., Carslaw, K., Dalvi, M., Edwards, J., Folberth, G. A., Gedney, N., Griffiths, P. T., Harper, A. B., Hendry, M. A., Hewitt, A. J., Johnson, B., Jones, A., Jones, C. D., Keeble, J., Liddicoat, S., Morgenstern, O., Parker, R. J., Predoi, V., Robertson, E., Siahaan, A., Smith, R. S., Swaminathan, R., Woodhouse, M. T., Zeng, G., and Zerroukat, M.: UKESM1: Description and evaluation of the UK Earth System Model, *Journal of Advances in Modeling Earth Systems*, 11, 4513–4558, <https://doi.org/10.1029/2019MS001739>, 2019.

800 805 Sellar, A. A., Walton, J., Jones, C. G., Wood, R., Abraham, N. L., Andrejczuk, M., Andrews, M. B., Andrews, T., Archibald, A. T., de Mora, L., Dyson, H., Elkington, M., Ellis, R., Florek, P., Good, P., Gohar, L., Haddad, S., Hardiman, S. C., Hogan, E., Iwi, A., Jones, C. D., Johnson, B., Kelley, D. I., Kettleborough, J., Knight, J. R., Köhler, M. O., Kuhlbrodt, T., Liddicoat, S., Linova-Pavlova, I., Mizielski, M. S., Morgenstern, O., Mulcahy, J., Neininger, E., O'Connor, F. M., Petrie, R., Ridley, J., Rioual, J. C., Roberts, M., Robertson, E., Rumbold, S., Seddon, J., Shepherd, H., Shim, S., Stephens, A., Teixiera, J. C., Tang, Y., Williams, J., Wiltshire, A., and Griffiths, P. T.: Implementation of U.K. Earth System Models for CMIP6, *Journal of Advances in Modeling Earth Systems*, 12, 1–27, <https://doi.org/10.1029/2019MS001946>, 2020.

810 815 Silva, R. A., West, J. J., Zhang, Y., Anenberg, S. C., Lamarque, J.-F., Shindell, D. T., Collins, W. J., Dalsoren, S., Faluvegi, G., Folberth, G., Horowitz, L. W., Nagashima, T., Naik, V., Rumbold, S., Skeie, R., Sudo, K., Takemura, T., Bergmann, D., Cameron-Smith, P., Cionni, I., Doherty, R. M., Eyring, V., Josse, B., MacKenzie, I. A., Plummer, D., Righi, M., Stevenson, D. S., Strode, S., Szopa, S., and Zeng, G.: Global premature mortality due to anthropogenic outdoor air pollution and the contribution of past climate change, *Environmental Research Letters*, 8, 034 005, <https://doi.org/10.1088/1748-9326/8/3/034005>, 2013.

820 825 Silva, R. A., West, J. J., Lamarque, J.-F., Shindell, D. T., Collins, W. J., Dalsoren, S., Faluvegi, G., Folberth, G., Horowitz, L. W., Nagashima, T., Naik, V., Rumbold, S. T., Sudo, K., Takemura, T., Bergmann, D., Cameron-Smith, P., Cionni, I., Doherty, R. M., Eyring, V., Josse, B., MacKenzie, I. A., Plummer, D., Righi, M., Stevenson, D. S., Strode, S., Szopa, S., and Zengast, G.: The effect of future ambient air pollution on human premature mortality to 2100 using output from the ACCMIP model ensemble, *Atmospheric Chemistry and Physics*, 16, 9847–9862, <https://doi.org/10.5194/acp-16-9847-2016>, 2016.

830 835 Staehle, C., Rieder, H. E., Fiore, A. M., and Schnell, J. L.: Technical note: An assessment of the performance of statistical bias correction techniques for global chemistry–climate model surface ozone fields, *Atmospheric Chemistry and Physics*, 24, 5953–5969, <https://doi.org/10.5194/acp-24-5953-2024>, 2024.

840 845 Stevenson, D. S., Young, P. J., Naik, V., Lamarque, J.-F., Shindell, D. T., Voulgarakis, A., Skeie, R. B., Dalsoren, S. B., Myhre, G., Berntsen, T. K., Folberth, G. A., Rumbold, S. T., Collins, W. J., MacKenzie, I. A., Doherty, R. M., Zeng, G., van Noije, T. P. C., Strunk, A., Bergmann, D., Cameron-Smith, P., Plummer, D. A., Strode, S. A., Horowitz, L., Lee, Y. H., Szopa, S., Sudo, K., Nagashima, T., Josse, B., Cionni, I., Righi, M., Eyring, V., Conley, A., Bowman, K. W., Wild, O., and Archibald, A.: Tropospheric ozone changes, radiative forcing and attribution to emissions in the Atmospheric Chemistry and Climate Model Intercomparison Project (ACCMIP), *Atmospheric Chemistry and Physics*, 13, 3063–3085, <https://doi.org/10.5194/acp-13-3063-2013>, 2013.

850 855 Stevenson, D. S., Zhao, A., Naik, V., O'Connor, F. M., Tilmes, S., Zeng, G., Murray, L. T., Collins, W. J., Griffiths, P. T., Shim, S., Horowitz, L. W., Sentman, L. T., and Emmons, L.: Trends in global tropospheric hydroxyl radical and methane lifetime since 1850 from AerChem-MIP, *Atmospheric Chemistry and Physics*, 20, 12 905–12 920, <https://doi.org/10.5194/acp-20-12905-2020>, 2020.

860 865 Stohl, A., Bonasoni, P., Cristofanelli, P., Collins, W., Feichter, J., Frank, A., Forster, C., Gerasopoulos, E., Gäggeler, H., James, P., Kentarchos, T., Kromp-Kolb, H., Krüger, B., Land, C., Meloen, J., Papayannis, A., Priller, A., Seibert, P., Sprenger, M., Roelofs, G. J., Scheel, H. E., Schnabel, C., Siegmund, P., Tobler, L., Trickl, T., Wernli, H., Wirth, V., Zanis, P., and Zerefos, C.: Stratosphere-

830 troposphere exchange: A review, and what we have learned from STACCATO, *Journal of Geophysical Research: Atmospheres*, 108, [https://doi.org/https://doi.org/10.1029/2002JD002490](https://doi.org/10.1029/2002JD002490), 2003.

835 Szopa, S., Naik, V., Adhikar, B., Artaxo, P., Berntsen, T., Collins, W., Fuzzi, S., Gallardo, L., Kiendler-Scharr, A., Klimont, Z., Liao, H., Unger, N., and Zanis, P.: Short-lived Climate Forcers in Climate Change 2021: The Physical Science Basis: Working Group I Contribution to the Sixth Assessment Report of the Intergovernmental Panel on Climate Change, pp. 817–922, Cambridge University Press, <https://doi.org/10.1017/9781009157896.008>, 2021.

840 Tarasick, D., Galbally, I. E., Cooper, O. R., Schultz, M. G., Aucellet, G., Leblanc, T., Wallington, T. J., Ziemke, J., Liu, X., Steinbacher, M., Staehelin, J., Vigouroux, C., Hannigan, J. W., García, O., Foret, G., Zanis, P., Weatherhead, E., Petropavlovskikh, I., Worden, H., Osman, M., Liu, J., Chang, K.-L., Gaudel, A., Lin, M., Granados-Muñoz, M., Thompson, A. M., Oltmans, S. J., Cuesta, J., Dufour, G., Thouret, V., Hassler, B., Trickl, T., and Neu, J. L.: Tropospheric Ozone Assessment Report: Tropospheric ozone from 1877 to 2016, observed levels, trends and uncertainties, *Elementa: Science of the Anthropocene*, 7, 39, <https://doi.org/10.1525/elementa.376>, 2019.

845 Turnock, S. T., Spracklen, D. V., Carslaw, K. S., Mann, G. W., Woodhouse, M. T., Forster, P. M., Haywood, J., Johnson, C. E., Dalvi, M., Bellouin, N., and Sanchez-Lorenzo, A.: Modelled and observed changes in aerosols and surface solar radiation over Europe between 1960 and 2009, *Atmospheric Chemistry and Physics*, 15, 9477–9500, <https://doi.org/10.5194/acp-15-9477-2015>, 2015.

850 Turnock, S. T., Wild, O., Dentener, F. J., Davila, Y., Emmons, L. K., Flemming, J., Folberth, G. A., Henze, D. K., Jonson, J. E., Keating, T. J., Kengo, S., Lin, M., Lund, M., Tilmes, S., and O'Connor, F. M.: The impact of future emission policies on tropospheric ozone using a parameterised approach, *Atmospheric Chemistry and Physics*, 18, 8953–8978, <https://doi.org/10.5194/acp-18-8953-2018>, 2018.

855 Turnock, S. T., Allen, R. J., Andrews, M., Bauer, S. E., Deushi, M., Emmons, L., Good, P., Horowitz, L., John, J. G., Michou, M., Nabat, P., Naik, V., Neubauer, D., O'Connor, F. M., Olivié, D., Oshima, N., Schulz, M., Sellar, A., Shim, S., Takemura, T., Tilmes, S., Tsigaridis, K., Wu, T., and Zhang, J.: Historical and future changes in air pollutants from CMIP6 models, *Atmospheric Chemistry and Physics*, 20, 14 547–14 579, <https://doi.org/10.5194/acp-20-14547-2020>, 2020.

Turnock, S. T., Reddington, C. L., West, J. J., and O'Connor, F. M.: The Air Pollution Human Health Burden in Different Future Scenarios That Involve the Mitigation of Near-Term Climate Forcers, *Climate and Land-Use, GeoHealth*, 7, e2023GH000812, <https://doi.org/https://doi.org/10.1029/2023GH000812>, e2023GH000812 2023GH000812, 2023.

855 United Nations Economic Commission for Europe: Clearing the Air: 25 years of the Convention on Long-Range Transboundary Air Pollution, <https://unece.org/sites/default/files/2021-06/25th%20year%20anniversary%20BOOKscreen.pdf>, 2004.

van Noije, T., Bergman, T., Le Sager, P., O'Donnell, D., Makkonen, R., Gonçalves-Ageitos, M., Döscher, R., Fladrich, U., von Hardenberg, J., Keskinen, J.-P., Korhonen, H., Laakso, A., Myriokefalitakis, S., Ollinaho, P., Pérez García-Pando, C., Reerink, T., Schrödner, R., Wyser, K., and Yang, S.: EC-Earth3-AerChem: a global climate model with interactive aerosols and atmospheric chemistry participating in CMIP6, *Geoscientific Model Development*, 14, 5637–5668, <https://doi.org/10.5194/gmd-14-5637-2021>, 2021.

860 Škerlak, B., Sprenger, M., and Wernli, H.: A global climatology of stratosphere–troposphere exchange using the ERA-Interim data set from 1979 to 2011, *Atmospheric Chemistry and Physics*, 14, 913–937, <https://doi.org/10.5194/acp-14-913-2014>, 2014.

865 Wang, H., Lu, X., Jacob, D. J., Cooper, O. R., Chang, K.-L., Li, K., Gao, M., Liu, Y., Sheng, B., Wu, K., Wu, T., Zhang, J., Sauvage, B., Nédélec, P., Blot, R., and Fan, S.: Global tropospheric ozone trends, attributions, and radiative impacts in 1995–2017: an integrated analysis using aircraft (IAGOS) observations, ozonesonde, and multi-decadal chemical model simulations, *Atmospheric Chemistry and Physics*, 22, 13 753–13 782, <https://doi.org/10.5194/acp-22-13753-2022>, 2022.

West, J. J., Szopa, S., and Hauglustaine, D. A.: Human mortality effects of future concentrations of tropospheric ozone, *Comptes Rendus Geoscience*, 339, 775–783, <https://doi.org/10.1016/j.crte.2007.08.005>, impact du changement climatique global sur la qualité de l'air à l'échelle régionale, 2007.

Wild, O. and Prather, M. J.: Global tropospheric ozone modeling: Quantifying errors due to grid resolution, *Journal of Geophysical Research: Atmospheres*, 111, [https://doi.org/https://doi.org/10.1029/2005JD006605](https://doi.org/10.1029/2005JD006605), 2006.

Wild, O., Fiore, A. M., Shindell, D. T., Doherty, R. M., Collins, W. J., Dentener, F. J., Schultz, M. G., Gong, S., MacKenzie, I. A., Zeng, G., Hess, P., Duncan, B. N., Bergmann, D. J., Szopa, S., Jonson, J. E., Keating, T. J., and Zuber, A.: Modelling future changes in surface ozone: a parameterized approach, *Atmospheric Chemistry and Physics*, 12, 2037–2054, <https://doi.org/10.5194/acp-12-2037-2012>, 2012.

Wild, O., Voulgarakis, A., O'Connor, F., Lamarque, J.-F., Ryan, E. M., and Lee, L.: Global sensitivity analysis of chemistry–climate model budgets of tropospheric ozone and OH: exploring model diversity, *Atmospheric Chemistry and Physics*, 20, 4047–4058, <https://doi.org/10.5194/acp-20-4047-2020>, 2020.

Xing, J., Wang, J., Mathur, R., Wang, S., Sarwar, G., Pleim, J., Hogrefe, C., Zhang, Y., Jiang, J., Wong, D. C., and Hao, J.: Impacts of aerosol direct effects on tropospheric ozone through changes in atmospheric dynamics and photolysis rates, *Atmospheric Chemistry and Physics*, 17, 9869–9883, <https://doi.org/10.5194/acp-17-9869-2017>, 2017.

Yan, Y., Pozzer, A., Ojha, N., Lin, J., and Lelieveld, J.: Analysis of European ozone trends in the period 1995–2014, *Atmospheric Chemistry and Physics*, 18, 5589–5605, <https://doi.org/10.5194/acp-18-5589-2018>, 2018.

Young, P. J., Archibald, A. T., Bowman, K. W., Lamarque, J.-F., Naik, V., Stevenson, D. S., Tilmes, S., Voulgarakis, A., Wild, O., Bergmann, D., Cameron-Smith, P., Cionni, I., Collins, W. J., Dalsøren, S. B., Doherty, R. M., Eyring, V., Faluvegi, G., Horowitz, L. W., Josse, B., Lee, Y. H., MacKenzie, I. A., Nagashima, T., Plummer, D. A., Righi, M., Rumbold, S. T., Skeie, R. B., Shindell, D. T., Strode, S. A., Sudo, K., Szopa, S., and Zeng, G.: Pre-industrial to end 21st century projections of tropospheric ozone from the Atmospheric Chemistry and Climate Model Intercomparison Project (ACCMIP), *Atmospheric Chemistry and Physics*, 13, 2063–2090, <https://doi.org/10.5194/acp-13-2063-2013>, 2013.

Young, P. J., Naik, V., Fiore, A. M., Gaudel, A., Guo, J., Lin, M. Y., Neu, J. L., Parrish, D. D., Rieder, H. E., Schnell, J. L., Tilmes, S., Wild, O., Zhang, L., Ziemke, J. R., Brandt, J., Delcloo, A., Doherty, R. M., Geels, C., Hegglin, M. I., Hu, L., Im, U., Kumar, R., Luhar, A., Murray, L., Plummer, D., Rodriguez, J., Saiz-Lopez, A., Schultz, M. G., Woodhouse, M. T., and Zeng, G.: Tropospheric Ozone Assessment Report: Assessment of global-scale model performance for global and regional ozone distributions, variability, and trends, *Elem Sci Anth*, 6, 10, <https://doi.org/10.1525/elementa.265>, 2018.

Zanis, P., Akritidis, D., Turnock, S., Naik, V., Szopa, S., Georgoulias, A. K., Bauer, S. E., Deushi, M., Horowitz, L. W., Keeble, J., Sager, P. L., O'Connor, F. M., Oshima, N., Tsigaridis, K., and van Noije, T.: Climate change penalty and benefit on surface ozone: A global perspective based on CMIP6 earth system models, *Environmental Research Letters*, 17, 024014, <https://doi.org/10.1088/1748-9326/ac4a34>, 2022.

Zeng, G., Morgenstern, O., Williams, J. H. T., O'Connor, F. M., Griffiths, P. T., Keeble, J., Deushi, M., Horowitz, L. W., Naik, V., Emmons, L. K., Abraham, N. L., Archibald, A. T., Bauer, S. E., Hassler, B., Michou, M., Mills, M. J., Murray, L. T., Oshima, N., Sentman, L. T., Tilmes, S., Tsigaridis, K., and Young, P. J.: Attribution of Stratospheric and Tropospheric Ozone Changes Between 1850 and 2014 in CMIP6 Models, *Journal of Geophysical Research: Atmospheres*, 127, e2022JD036452, [https://doi.org/https://doi.org/10.1029/2022JD036452](https://doi.org/10.1029/2022JD036452), e2022JD036452 2022JD036452, 2022.

Zhang, J., Furtado, K., Turnock, S. T., Mulcahy, J. P., Wilcox, L. J., Booth, B. B., Sexton, D., Wu, T., Zhang, F., and Liu, Q.: The role of anthropogenic aerosols in the anomalous cooling from 1960 to 1990 in the CMIP6 Earth system models, *Atmospheric Chemistry and Physics*, 21, 18 609–18 627, <https://doi.org/10.5194/acp-21-18609-2021>, 2021.

Zhang, Y., Cooper, O. R., Gaudel, A., Thompson, A. M., Nédélec, P., Ogino, S.-Y., and West, J. J.: Tropospheric ozone change from 1980 to
905 2010 dominated by equatorward redistribution of emissions, *Nature Geoscience*, 9, 875–879, <https://doi.org/10.1038/ngeo2827>, 2016.